

Evidence for a Gradual Decline in the Universal Rest-Frame UV Luminosity Density for $z < 1$

Lennox L. Cowie^{1,2}, Antoinette Songaila & Amy J. Barger^{1,2}

Institute for Astronomy, University of Hawaii, 2680 Woodlawn Drive, Honolulu, HI 96822

To be published in *Astronomical Journal*, August 1999

ABSTRACT

We have utilized various magnitude-limited samples drawn from an extremely deep and highly complete spectroscopic redshift survey of galaxies observed in seven colors in the Hawaii Survey Fields and the Hubble Deep Field to investigate the evolution of the universal rest-frame ultraviolet luminosity density from $z = 1$ to the present. The multi-color data (U' , B , V , R , I , J , HK') enable the sample selection to be made in the rest-frame ultraviolet for the entire redshift range. Due to the large sample size and depth ($U_{AB} = 24.75$, $B_{AB} = 24.75$, $I_{AB} = 23.5$), we are able to accurately determine the luminosity density to $z = 1$. We do not confirm the very steep evolution reported by Lilly et al. (1996) but instead find a shallower slope, approximately $(1 + z)^{1.5}$ for $q_0 = 0.5$, which would imply that galaxy formation is continuing smoothly to the present time rather than peaking at $z = 1$. Much of the present formation is taking place in smaller galaxies. Detailed comparisons with other recent determinations of the evolution are presented.

Subject headings: galaxies: evolution – galaxies: formation – galaxies:luminosity function

¹Visiting astronomer, W. M. Keck Observatory, jointly operated by the California Institute of Technology and the University of California.

²Visiting Astronomer, Canada-France-Hawaii Telescope, operated by the National Research Council of Canada, the Centre National de la Recherche Scientifique of France and the University of Hawaii.

1. Introduction

Over the past several years it has become widely accepted that the global star formation rate — at least as seen in the optical and ultraviolet light — had a strong peak at around $z = 1$ and then fell very steeply at lower redshifts (e.g. Pozzetti, Madau & Dickinson 1998 and references therein). This would mean that most of the integrated total star formation producing optically visible light would have occurred at roughly half the present age of the Universe. However, the argument for the steep fall-off at $z < 1$ relies on a single important analysis by Lilly et al. (1996) based on the Canada France Redshift Survey (CFRS) sample. This sample has two weaknesses when it is used to determine the evolution of rest-frame UV light. The first of these is that it is a red (I band) selected sample with V and I photometry, primarily, and only partial B and K coverage. At low redshifts this requires a very substantial extrapolation across the 4000 Å break to obtain a 2800 Å rest-frame luminosity. The second weakness is that the CFRS is slightly too shallow for this problem ($I_{AB} = 22.5$, or $I \sim 22.1$ in the Kron-Cousins system). At the highest redshifts, near $z = 1$, the sample does not probe deep enough in the luminosity function to allow a reliable extrapolation to a total luminosity density.

In this paper we utilize a large, extremely deep, and highly complete spectroscopic redshift survey of galaxies observed in seven colors (U' [3400 ± 150 Å], B , V , R , I , J , HK' ; the limits in the blue and red are $B_{AB} = 24.75$ and $I_{AB} = 23.5$, respectively) in the Hawaii Survey Fields and the Hubble Deep Field to investigate the rest-frame UV luminosity density evolution from $z = 1$ to the present. With this sample we are able to avoid the above problems encountered in the CFRS study. First, the availability of both ultraviolet and blue data means that we can *select* objects based on their rest-frame ultraviolet magnitudes at all redshifts and hence avoid the serious problem of selecting at redder wavelengths and extrapolating to obtain the UV colors. Second, the substantial additional depth of our sample allows us to probe to the flat segments of the luminosity function, thereby giving a more accurate determination of the luminosity density function. It also enables us to extend the results to redshifts beyond $z = 1$. This uniform sample selection strongly minimises possible errors due to dust in the galaxies, unless there is substantial evolution of galaxy dust properties with redshift. Thus, the shape of the present UV luminosity density evolution should be an accurate representation of the shape of the star formation history to within the one residual uncertainty of differential dust evolution.

We find that the $z < 1$ UV luminosity density falls with a shallower slope — roughly $(1+z)^{1.5}$ for $q_0 = 0.5$ — than reported by Lilly et al. (1996). Our low redshift UV luminosity density value is considerably higher than that found by Lilly et al. and agrees with the local UV luminosity density recently determined by Treyer et al. (1998). Consequently, much of

the integrated total of optically visible stars is still being assembled at the present time.

The outline of the paper is as follows. In §2 we provide a brief, self-contained analysis of the distribution of light with redshift in the Hubble Deep Field. If this small field is representative, then the analysis can be used to demonstrate the primary conclusion of the paper, namely that the fall-off in the rest-frame ultraviolet luminosity density below $z = 1$ is relatively shallow. We then proceed to the main analysis. We discuss the data in §3; the photometry and the statistical and systematic errors are presented in an Appendix for textual clarity. In §4 we construct the rest-frame ultraviolet luminosity functions and the UV luminosity density as a function of redshift. We then present comparisons with the results of other analyses. In order to be fully self-consistent, we specifically restrict ourselves to the evolution of the ultraviolet luminosity density and do not attempt to compare with studies of emission-line evolution. In §5 we briefly summarize our conclusions.

2. Preliminary Digression

The Hubble Deep Field (HDF; Williams et al. 1996) provides our deepest view of the faint galaxy populations. The color information in the HDF has been extensively used to estimate the high- z star formation history of optically-selected galaxies (e.g. Madau et al. 1997; Connolly et al. 1997; Sawicki, Lin & Yee 1997). As large numbers of spectroscopic redshifts have accumulated for HDF galaxies (Steidel et al. 1996; Cohen et al. 1996; Lowenthal et al. 1997; Phillips et al. 1997; Songaila 1997; Barger et al. 1999), it is now possible to use these spectroscopic data to examine the history of star formation at $z < 1$ and to show directly that, within the HDF itself, a substantial fraction of the star formation is occurring at low redshift. A similar conclusion is reached by Pascarelle et al. (1998) based on a very different photometric redshift analysis.

The sky surface brightness of the integrated galaxy light computed from the Williams et al. objects in the deeper areas of the WFC chips — an area of 4.9 arcmin^2 — is shown by the solid line in Figure 1. There are 96 objects in this region of the HDF that now have spectroscopic identifications. These identified objects, which are generally the brighter galaxies, contain most of the optical and roughly half of the 3000 \AA light. We have subdivided the contributions by redshift, showing the light from known $z < 1$ galaxies as the solid boxes and that from known $z < 0.5$ galaxies as solid diamonds. The dashed line, which shows the combined light from all known $z > 1$ galaxies and *all* unidentified or unobserved objects, represents an extreme upper bound to the fraction of light arising from galaxies at $z > 1$.

Since some (possibly substantial) fraction of the fainter unidentified galaxies will lie at

$z < 1$, the ratio of the $z > 1$ light to that at lower redshift is overestimated here but can already be used to make the argument that a large fraction of star formation is local. As was pointed out in Cowie (1988), Songaila et al. (1990), and Madau et al. (1997), the integrated massive star formation, which can be characterized by the local metal density, is directly proportional to the observed-frame ultraviolet sky brightness, independent of cosmology, through the relation

$$\rho_{\text{metals}} = \frac{4\pi S_{\nu}}{\varepsilon c} \quad (1)$$

Estimates of the normalizing factor ε can be found in Songaila et al. (1990) and Madau et al. (1997). Applying this relation to the 3000 Å light in Figure 1, we see immediately that comparable amounts of metals have been produced by $z < 0.5$ galaxies and by $z > 1$ galaxies, since the ultraviolet sky brightness of the known $z < 0.5$ galaxies is already 54% of the maximum possible $z > 1$ light. However, in this simple form, the argument depends on the assumption that the light from star-forming galaxies is roughly flat in f_{ν} .

A more conservative approach is to compare the known $z < 0.5$ 3000 Å light with the possible $z > 1$ 6020 Å light. This comparison at equivalent rest-frame wavelengths allows for the shapes of the spectral energy distributions (SEDs) and for dust extinction. It also takes into account the disappearance of very high redshift galaxies from the 3000 Å band. The ratio $R_{SF} \equiv \text{light}(z < 0.5)/\text{light}(z > 1)$ from Figure 1 is then 26%. This represents a very extreme lower bound on the ratio of the integrated star formation at $z < 0.5$ to that at $z > 1$.

The implications for the evolution of the low- z SFR $[\dot{\rho}_*(z)]$ can be shown with the simple model

$$\begin{aligned} \dot{\rho}_*(z) &= A(1+z)^{\alpha} \quad , \quad z < 1 \\ &= 2^{\alpha} A \quad , \quad z > 1 \end{aligned} \quad (2)$$

that can be integrated analytically. For $q_0 = 0.5$ $R_{SF} = 18\%$ for $\alpha = 4$, 30% for $\alpha = 3$ and 48% for $\alpha = 2$. Thus, even comparing the *candidate* $z > 1$ visual light with the *known* $z < 0.5$ ultraviolet light requires $\alpha \ll 3.2$. Provided only that the small HDF is a representative field, even the very conservative and extremely robust version of the argument requires a shallower slope than has been inferred from the CFRS data (*viz.*, 3.9 ± 0.75). The remainder of the paper verifies this conclusion using our wide-field ultraviolet and optically-selected samples.

3. Data Sets

The primary data sets used in the present study are two $6' \times 2.5'$ areas crossing the HDF and the Hawaii Survey Field SSA22 (Lilly, Cowie & Gardner 1991). In each case the

field has been imaged in 7 colors — U' ($3400 \pm 150 \text{ \AA}$), B , V , R , I , J and HK' — where R and I are Kron-Cousins and the HK' ($1.9 \pm 0.4 \mu$) filter is described in Wainscoat & Cowie (in preparation). The images were obtained on the Keck II telescope using LRIS (Oke et al. 1995) and on the University of Hawaii 2.2m and the Canada-France-Hawaii 3.6m telescopes using QUIRC (Hodapp et al. 1996), ORBIT, and the UH8K CCD Mosaic Camera built by Metzger, Luppino, and Miyazaki. The fields, whose sizes were set by the usable LRIS area, are fully covered in all colors. All magnitudes were measured in $3''$ diameter apertures and corrected to total magnitudes following the procedures in Cowie et al. (1994). A further two similarly sized areas covering the Hawaii Survey Fields SSA4 (Cowie et al. 1994) and SSA13 (Lilly, Cowie & Gardner 1991) with B, V, I, HK' data were used to augment the SSA22 and HDF B , I , and HK' -selected samples. The fields, areas, magnitude limits, and numbers of spectroscopically-identified galaxies, stars, and unknowns (unobserved or unidentified objects) for each of the color-selected samples are given in Table 1. A more detailed discussion and analysis of the photometric and spectroscopic samples used in this paper can be found in Barger et al. (1999).

4. Rest-Frame Ultraviolet Luminosity Density Evolution

4.1. Construction of the luminosity functions

For redshifts, z , for which the rest-frame UV wavelength, λ_U , maps directly to the wavelength of one of the observed color bands, the absolute rest-frame UV magnitude, M_U , in the AB system ($M_U = 0$ corresponds to $\log_{10} F_\nu = -48.57$) is given by

$$M_U = m_{AB} + 2.5 \log_{10}(1 + z) - 5 \log_{10}(d_L(z)/10 \text{ pc}) \quad (3)$$

where m_{AB} is the observed magnitude at the redshifted wavelength $\lambda_U(1 + z)$ in the AB system and $d_L(z)$ is the luminosity distance. For redshifts such that $\lambda_U(1 + z)$ differs by a small amount from this central wavelength, we can apply the same formula but with the addition of a small differential k correction $dk(z)$, defined as

$$dk(z) = -2.5 \log_{10} \frac{f_\nu(\lambda_U(1 + z))}{f_\nu(\lambda_U(1 + z_C))} \quad (4)$$

where f_ν is the SED of the galaxy, and z_C is the redshift corresponding to the center of the band. Because of the frequent, regularly-spaced color sampling, we can simply construct $dk(z)$ by interpolation from the neighboring color bands. The value of $dk(z)$ is generally small (less than 0.2 mag) for the redshift intervals which are used.

The 2500 \AA rest-frame absolute magnitudes, computed in the appropriate redshift intervals from the U' , B , V and I samples, are shown versus redshift in Figure 2. In the

overlapping redshift intervals the absolute magnitudes compare well. The rise in the maximum absolute UV rest-frame luminosity with redshift mapped by the upper envelope of the distribution is partly a reflection of the larger volume sampled at high redshift but also partly reflects the known evolution that causes the maximum UV luminosity to increase with redshift (Lilly et al. 1996; Cowie et al. 1996); we will discuss this in more detail below.

We adopt the traditional V_{max} method of Felten (1977) for constructing the luminosity functions. The number density of galaxies in the redshift range $[z_1, z_2]$ with magnitude M is given by

$$\phi(M) dM \propto \sum \frac{1}{V_{max}(M)} \quad (5)$$

where the sum is over all galaxies with magnitude $M \pm dM/2$. $V_{max}(M)$ is the maximum total volume in all the samples where galaxies with absolute magnitude M are observable in the appropriate apparent magnitude range and lie in the redshift range. (A very complete description of the procedure may be found in Ellis et al. 1996). The ultraviolet luminosity density, ℓ , is then

$$\ell = 4.4 \times 10^{20} \sum \frac{10^{-0.4M}}{V_{Max}(M)} \text{ ergs s}^{-1} \text{ Hz}^{-1} \quad (6)$$

where the sum is over all the observed objects. We use Schechter function fits with $\alpha = -1$ to extend ℓ from the brighter absolute magnitudes observed to $M = -16$, which we then use as our total luminosity density.

In the computation of the luminosity functions, we assign errors based on the Poisson distribution corresponding to the number of galaxies contributing to the absolute magnitude bin. However, a larger potential source of error is the missing or unidentified galaxies in each sample. Following the standard procedure, we compute the luminosity function after assuming that these objects follow the redshift distribution of the identified objects, but because of systematic effects, this assumption may not be valid. We have therefore also computed the LFs with all, and also with none, of the missing objects allocated into the redshift bin, which should provide extremal estimates of this error. In the case where we allocated the missing objects into the redshift bin, the allocated redshifts were randomly distributed uniformly within the redshift interval. We are able to use this very robust procedure because of the extremely high completeness of the spectroscopic samples.

4.2. UV luminosity functions versus rest wavelength

A key issue is the optimum wavelength at which to compute the rest-frame LFs and the UV light densities. Previous efforts, such as those by the CFRS, have computed the

light densities at a relatively long wavelength of 2800 Å, which is optimal for a red sample and minimises dust extinction but may be a poorer measure of massive star formation rates than shorter wavelengths. The local UV sample of Treyer et al. (1998), which provides an invaluable low redshift comparison, is at 2000 Å. However, our own sample gives the best combination of wide redshift range and largest galaxy sample at a rest wavelength around 2500 Å.

In the following discussion we shall use all three of these rest wavelengths for specific comparisons and analyses. Before proceeding, however, we use the various color samples to show that at $z = 1$ the luminosity functions and light densities are only weakly sensitive to the wavelength choice. At $z = 1$ the U' , B and V samples correspond to rest-wavelengths of 1700 Å, 2250 Å and 2750 Å. In Figure 3 we compare the luminosity functions constructed at each of these rest wavelengths in the redshift interval $0.7 < z < 1.3$. It is apparent that the luminosity functions are quite similar, with only a slight fading of M_U with decreasing wavelength. The corresponding luminosity densities for galaxies with luminosities greater than $M_U = -17.5$ (squares), or extrapolated to $M = -16$ assuming an $\alpha = -1$ Schechter function (dashed line), are shown in Figure 4. The total UV luminosity density above $M = -16$ in this redshift interval is fit by a power law

$$\ell = 2.6 \times 10^{26} h_{65} \left(\frac{\lambda}{3000 \text{ Å}} \right)^{1.1} \text{ ergs Mpc}^{-3} \text{ Hz}^{-1} \quad (7)$$

where h_{65} is the Hubble constant in units of $65 \text{ km s}^{-1} \text{ Mpc}^{-1}$. We shall generally avoid comparing light densities at different wavelengths. Where necessary, however, we use the weak wavelength dependence of equation (7), assuming, somewhat arbitrarily, that this is valid for other redshifts.

4.3. The redshift evolution of the 2500 Å rest-frame luminosity density

We first construct the 2500 Å rest-frame luminosity function in three redshift bands: $z = 0.20 - 0.50$ using the U' -selected sample (Figure 5), $z = 0.6 - 1.0$ using the B -selected sample (Figure 6), and $z = 1.0 - 1.5$ using the V -selected sample (Figure 7). In each case the solid curve is the incompleteness-corrected luminosity function with $\pm 1 \sigma$ Poisson error bars on the symbols; the dotted curve is the luminosity function obtained from only the observed objects (the minimal function); and the dashed curve is the luminosity function when all the unidentified objects are taken to lie within the redshift interval (the maximal function).

We next compute the luminosity density for galaxies more luminous than $M_U = -16$. This is a directly determined quantity in the lowest redshift interval, but for the higher

redshift intervals it requires an extrapolation which was made with an $\alpha = -1$ Schechter function fit. For $z = 0.6 - 1.0$ the observed light density for $M_{AB} \leq -17.5$ is $1.7 \times 10^{26} h_{65} \text{ ergs s}^{-1} \text{ Hz}^{-1} \text{ Mpc}^{-3}$, and the extrapolated light density is 21% higher. For $z = 1.0 - 1.5$ the observed light density for $M_{AB} \leq -18.25$ is $1.4 \times 10^{26} h_{65} \text{ ergs s}^{-1} \text{ Hz}^{-1} \text{ Mpc}^{-3}$, and the extrapolated light density is 34% higher.

The incompleteness-corrected $M_{AB} \leq -16$ light density as a function of redshift is shown in Figure 8 as the filled squares; the redshift range is shown as the thin horizontal lines. The statistical and systematic errors (see Appendix) are shown as the thicker portions of the error bar. We have performed similar calculations for both the minimal and maximal functions. These represent the extremal range of the possible light density at a given redshift and are shown as the open squares joined by the vertical thin lines. The solid line shows a simple $(1+z)^{1.5}$ evolution law which would result in equal amounts of star formation per unit redshift interval and would constitute an acceptable fit to the data. The dashed line shows a redshift evolution of $(1+z)^4$ matched to the second data point; this is clearly too steep, even allowing for the maximum incompleteness correction.

The shape and normalization of the rest-frame UV luminosity function is of course a consequence of a complex mix of the evolution of the star formation rates in galaxies of various types and masses and the decrease in M_{U*} with declining redshift, which most likely reflects a preferential drop in the star formation rates of the most massive galaxies (Cowie et al. 1996). Nevertheless, it is interesting to compare the functions to determine if there is evidence for a change of shape (Figure 9). For $q_0 = 0.5$ the functions can be quite well overlayed with a simple shift in the absolute magnitude (pure luminosity evolution). Though there is a hint that the higher redshift functions might be steeper, there is no statistically significant difference in the shapes as a function of redshift. The absolute magnitude shifts used in constructing Figure 9 (+0.65 mag at $z = 0.6 - 1.0$ and +0.75 mag at $z = 1.0 - 1.5$, both relative to $z = 0.2 - 0.5$) can also be used to check the 2500 Å rest-frame luminosity density evolution and would imply a ratio of 1 : 1.8 : 2.0 in these redshift bins; the best-fit power law corresponds to $\ell \propto (1+z)^{1.4}$, which is quite similar to the estimates given above.

4.4. Comparison with other samples

The most directly comparable sample is the low-redshift, rest-frame ultraviolet (2000 Å) selected sample of Treyer et al. (1998). To make a direct comparison with this sample we have computed the 2000 Å luminosity functions at $z = 0.5 - 0.9$ using the U' -selected sample and at $z = 1.0 - 1.5$ using the B -selected sample. We compare these with the luminosity function determined by Treyer et al. in Figures 10 and 11. The solid line with the symbols

shows the presently-determined luminosity function. The dashed line shows the Treyer et al. function for $H_0 = 65 \text{ km s}^{-1} \text{ Mpc}^{-1}$ and converting the magnitude system used by Treyer et al. to AB magnitudes with a 2.29 mag offset. Here we have used a renormalization rather than a magnitude offset to overlay the functions. For $z = 0.5 - 0.9$ the normalization of the Treyer et al. function is multiplied by 1.7. For $z = 1.0 - 1.5$ the normalization is multiplied by 2.8. The corresponding luminosity density changes would be an increase of $\ell \propto (1+z)^{1.3}$.

The measured 2000 Å luminosity densities in the Treyer et al. sample are compared with the incompleteness-corrected 2000 Å luminosity densities from this work in Figure 12, where once again we have shown the maximal and minimal luminosity densities with open squares. As was the case for the 2500 Å data, the combined data sets exhibit a slow evolution, as shown by the $(1+z)^{1.5}$ solid line. A steeper dependence, such as the $(1+z)^4$ evolution of the dashed line, is radically inconsistent with the data. Because of the steep rise in the Treyer et al. luminosity function at the faintest magnitudes, it is best fit by an $\alpha = -1.6$ power law rather than the $\alpha = -1.0$ power law (characteristic of the optical luminosity functions) which we have adopted in extrapolating the luminosity functions to the fainter magnitudes. In order to investigate the dependence on α we have fitted the 2000 Å luminosity functions at $z = 0.5 - 0.9$ and $z = 1 - 1.5$ with Schechter functions with indices $\alpha = -1.0$ and $\alpha = -1.5$. The fitted parameters and the luminosity densities above -16 are summarized in Table 2 where they are compared with the values derived by Treyer et al. Increasing the index from -1.0 to -1.5 has the effect of preferentially increasing the luminosity density at the higher redshifts where the extrapolation is larger. However, the effect is not large. Using the -1.5 derived luminosity density would increase the slope to $(1+z)^{1.7}$ from $(1+z)^{1.3}$ for the $\alpha = -1.0$ case.

We next compare the present sample with the Lilly et al. (1996) analysis of the CFRS data at a rest-frame wavelength of 2800 Å. In order to make the most direct comparison possible, we followed the Lilly et al. redshift intervals of $[0.2, 0.5]$, $[0.5, 0.75]$, $[0.75, 1]$, constructing the luminosity functions with the U' sample, the B sample, and the V sample, respectively. The luminosity densities constructed from these samples are shown in Figure 13, where the filled squares are again the incompleteness-corrected luminosity density, the thicker portions of the error bars show the systematic and statistical errors, and the open squares show the minimal and maximal light densities. The open diamonds show the Lilly et al. analysis; their three higher redshift points are based on the CFRS data and the lowest redshift point is based on the data of Loveday et al. (1992). The lowest redshift point is already contradicted by Treyer et al.’s (1998) analysis, shown as the filled diamond, corrected upwards by a factor of 1.5 for the wavelength difference between 2000 Å and 2800 Å. The Treyer et al. point is also comparable with the $[0.2, 0.5]$ Lilly point. The present data exhibit a much shallower slope than the Lilly et al. data in the $z = 0.2 - 1$ range. This results primarily

from the $[0.75, 1]$ point being about a factor of two lower than the highest redshift Lilly point. The two intermediate redshift points agree well with the CFRS analysis.

We also compare with the analyses of Connolly et al. (1997) and Sawicki et al. (1997), shown as open triangles and inverted open triangles, respectively, in Figure 13. These two analyses are based on photometrically estimated redshifts in the small HDF proper and are in broad general agreement with each other and with the work of Pascarelle et al. (1998). (We do not include a direct comparison to the latter work here as it is computed at 1500 \AA .) Following the discussion in the Appendix, we have made a small 20% downward correction to allow for the slightly higher counts in the relevant magnitude range in the HDF proper versus the wide surrounding field. Both the $[0.5, 1]$ and $[1.0, 1.5]$ points from these analyses are higher than our incompleteness-corrected estimate but are consistent within the statistical and incompleteness errors. Our best estimate value may indeed be slightly low here, since there may be preferential incompleteness in these redshift ranges. However, there is also relatively little validation of photometrically estimated redshifts in the range $z = 1$ to 2 where the observed spectral range ($\lambda = 3000 \text{ \AA}$ to $22,000 \text{ \AA}$) is quite featureless for blue galaxies. Thus, the high redshift Connolly et al. and Sawicki et al. points could be overestimated if lower redshift blue irregulars have been assigned to the wrong bin. Since our maximal incompleteness-corrected estimate is not substantially different from the photometrically estimated values, the discussion of §5 does not depend on the resolution of this issue.

4.5. The relative evolution of the rest-frame UV, blue and red light

As has been known for several years now (Lilly et al. 1996; Cowie et al. 1996) the rest-frame red luminosity has an extremely weak evolution with redshift out to $z = 1$. This slow evolution can be clearly seen in Figure 14, in which we compare the rest-frame 8000 \AA luminosity at $z = 0.2 - 0.5$, obtained using the I -selected sample, with that at $z = 0.7 - 1.3$, computed using the K -selected sample. The two functions can be brought into full consistency with a very small (0.2 mag) pure luminosity shift corresponding to a decrease of only 20% in the red light from $z = 0.8$ to $z = 0.35$, thereby confirming with the present sample that the downward evolution of the UV light density by a factor of two between $z = 1$ and $z = 0.35$ does take place against an essentially invariant shape and normalization for the red light density.

5. Summary

We have investigated the evolution of the universal ultraviolet luminosity density from $z = 1$ to the present using a magnitude-limited sample selected on the basis of rest-frame ultraviolet colors at all redshifts from an extremely deep and highly complete spectroscopic redshift survey. Our uniform selection procedure avoids the serious problem of selecting the sample at redder wavelengths and then extrapolating to obtain ultraviolet colors, and it strongly minimises possible errors due to dust in the galaxies, unless there is substantial evolution of galaxy dust properties with redshift. The depth of the current sample is also sufficiently deep to probe to the flat segments of the luminosity function and to extend the results to redshifts beyond $z = 1$, thereby enabling us to make an accurate determination of the luminosity density function.

We find that our incompleteness-corrected rest-frame 2500 Å luminosity densities for $M_U \leq -16$ as a function of redshift are well fit by an $l \propto (1 + z)^{1.5}$ evolution law for $q_0 = 0.5$. (The slope would be shallower for open geometries.) The decline in M_U with decreasing redshift most likely reflects a preferential drop in the star formation rates of the most massive galaxies. A direct comparison of the measured low-redshift 2000 Å luminosity density of Treyer et al. (1998) with incompleteness-corrected 2000 Å luminosity densities computed from our sample also shows that the slow evolution law of $l \propto (1 + z)^{1.5}$ provides a good fit. When we compare the Lilly et al. (1996) CFRS analysis with our sample analyzed at rest-frame 2800 Å, we find that our sample gives a much shallower slope in the $z = 0.2 - 1$ range. This most probably arises in part due to the relatively large extrapolation at low redshifts Lilly et al. needed to make to go from a primarily V and I -based data sample to ultraviolet colors. The two lowest-redshift Lilly et al. points are also in disagreement with the Treyer et al. analysis. Interestingly, however, the present UV luminosity density analysis leads to a closer agreement with star formation rates found in an $H\alpha$ analysis of the CFRS data by Tresse & Maddox (1998).

We can summarise our results in the form of the widely-discussed plot of UV luminosity density versus redshift, our version of which is shown for the 2500 Å rest frame in Figure 8 and at 2000 Å in Figure 12. This plot is rather different from the now conventional ‘Madau’ form which has a strong rise to $z = 1$. Rather, we see a fairly slow decline in $\dot{\rho}_{UV}$ from $z = 1.5$ to $z = 0$, which is reasonably well described by a simple $\dot{\rho}_{UV} = 7 \times 10^{25} (1 + z)^{1.5}$ ergs s⁻¹ Mpc⁻³ Hz⁻¹ relation. This result has fairly profound philosophical implications in that the integrated star formation is continuing to rise smoothly at the present time and the bulk of the star formation has occurred at recent times. (This result holds irrespective of cosmological geometry.) Put succinctly, as seen in the optical, now may be the epoch of galaxy formation and not $z = 1$.

A. Systematic and Statistical Errors and Comparison with HDF Photometry and Number Counts

Because much of our information on the $z > 1$ rest-frame UV luminosity density is based on the small Hubble Deep Field, it is important to check the consistency of the photometry and number counts between the present data and the HDF tables of Williams et al. (1996).

Since the wide-field area around the HDF fully overlaps the HDF proper, we can compare the photometric systems directly. We first identified the corresponding objects in the two tables whose centroids lie within $0''.4$ of each other and are not complex objects. We then compared our corrected aperture magnitudes with the total magnitudes in Williams et al. The color equations for the four bands are found to be,

$$\begin{aligned}
 I &= -0.39 + AB_{814} - 0.09(AB_{602} - AB_{814}) \\
 V &= 0.16 + AB_{602} + 0.40(AB_{602} - AB_{814}) \\
 V &= 0.14 + AB_{602} + 0.47(AB_{450} - AB_{602}) \\
 B &= 0.05 + AB_{450} \\
 U &= 0.10 + AB_{300} - 0.25(AB_{300} - AB_{450})
 \end{aligned} \tag{A1}$$

where we have forced the color term in the B equation to zero. Allowing for the offsets in zero points between the color systems ($I - I_{AB} = -0.33$, $B - B_{AB} = 0.16$), we can see that there is a maximum deviation of 0.15 mag in the V -band versus AB_{602} , where the color term is, however, large. We take this to be the maximum systematic uncertainty in the photometry.

Using these photometric transformations we next constructed the V -band number counts (galaxies and stars) in the WFPC areas of the HDF itself (4.9 arcmin^2) and in the 81 arcmin^2 area of the HDF flanking field region. This comparison is shown in Figure 15. There is broad general agreement in the counts within the small number fluctuations. Over the range, $21 < V < 24.25$, the HDF proper has a 17% higher total flux per unit area than the large flanking field area. In Figure 16 we show the HDF galaxy counts in B compared with the average B galaxy counts in the regions of the HDF and SSA22 used in the present analysis. (Only spectroscopically confirmed stars have been removed from both counts.) The total flux per unit area of objects in the HDF with $21 < B < 24.75$ is 13% higher than in the average of the two fields.

Finally, in Figure 17 we show a comparison of the total HDF $0 < z < 0.5$ and $0 < z < 1$ HDF sky surface brightness in the ranges $21 < V < 24.5$, $21 < B < 24.75$ and $21 < U' < 24.5$ with the present samples. In the analysis the HDF lies about 25% higher in the total light in this range, with a disproportionately high amount of $z < 0.5$ light, which is between 25% and 50% higher in the various colors. The results emphasize that clustering can cause

fluctuations at this level in fields of the size of the HDF, and they emphasize the importance of using multiple large areas. In order to compare with the HDF-derived data of Connolly et al. (1997) we have therefore revised their fluxes downward by 20%. However, the systematic error in the present much larger data sample should be considerably smaller than this and is dominated by the photometric errors. We will adopt a conservative systematic error limit of $\pm 20\%$ of the rest-frame UV luminosity densities.

In order to obtain a realistic estimate of the statistical error we divided the B sample into two parts — one comprising the HDF and SSA22 data and one comprising the SSA13 and SSA4 data — and constructed the rest-frame 2500 Å luminosity function in the $0.6 < z < 1$ range from each subsample. The two luminosity functions are shown in Figure 18. The luminosity densities inferred from the two functions differ by 17%. Based on this comparison, we have assigned a statistical error of $0.2 (N/40)^{-0.5}$, where N is the total number of galaxies in the sample bin, and we have added this error in quadrature to the systematic error to determine the formal error bars in the rest-frame UV luminosity density plot.

REFERENCES

- Barger, A.J., Cowie, L.L., Trentham, N., Fulton, E., Hu, E.M., Songaila, A., Hall, D. 1999, AJ117, 102
- Cohen, J.G., Cowie, L.L., Hogg, D.W., Songaila, A., Blandford, R., Hu, E.M., Shopbell, P. 1996, ApJ, 471, L5
- Connolly, A.J., Szalay, A.S., Dickinson, M., SubbaRao, M.U., Brunner, R.J. 1997, ApJ, 486, L11
- Cowie, L. L. 1988, in The post-recombination universe, Proceedings of the NATO Advanced Study Institute, Cambridge, UK, (Dordrecht: Kluwer), 1
- Cowie, L.L., Gardner, J.P., Hu, E.M., Songaila, A., Hodapp, K.-W., Wainscoat, R.J. 1994, ApJ, 434, 114.
- Cowie, L. L., Songaila, A., Hu, E. M., & Cohen, J. G. 1996, AJ 112, 839.
- Ellis, R.S., Colless, M., Broadhurst, T., Heyl, J., Glazebrook, K. 1996, MNRAS, 280, 235
- Felten, J.E. 1977, AJ82, 861
- Hodapp, K.-W., et al. 1996, New Astronomy 1, 177
- Lilly, S.J., Cowie, L.L., Gardner, J.P. 1991, ApJ, 369, L79
- Lilly, S.J., LeFèvre, O., Hammer, F., Crampton, D. 1996, ApJ, 460, L1
- Loveday, J., Peterson, B.A., Efstathiou, G., Maddox, S.J. 1992, ApJ, 390, 338
- Lowenthal, J., et al. 1997, ApJ, 481, 673
- Oke, B., et al. 1995, PASP, 107, 375
- Pascarelle, S. M., Lanzetta, K. M. & Fernandez-Soto, A. 1998, ApJ 508, L1.
- Phillips, A.C., et al. 1997, ApJ, 489, 543
- Sawicki, M. J., Lin, H. & Yee, H. K. C. 1997, AJ 113, 1.
- Songaila, A., Cowie, L.L., Lilly, S.J. 1990, ApJ, 348, 371
- Songaila, A. 1997, <http://www.ifa.hawaii.edu/~cowie/tts/tts.html>
- Steidel, C.C., Giavalisco, M., Dickinson, M., Adelberger, K. 1996, AJ, 112, 352
- Tresse, L., Maddox, S.J. 1998, ApJ, 495, 691
- Treyer, M.A., Ellis, R.S., Milliard, B., Donas, J., Bridges, T.J. 1998, MNRAS, 300, 303
- Williams, R., et al. 1996, AJ112, 1335

Table 1. Color-selected Samples

Color	Field	Area (arcmin ²)	Limit	Galaxies	Stars	Unknowns
U'	SSA22	15.7	$U' < 24.75$	115	12	6
	HDF	17.6	$U' < 24.5$	103	10	29
B	SSA22	16.0	$B < 24.75$	166	35	14
	HDF	13.6	$B < 24.25$	109	14	25
	SSA13	12.7	$B < 24.25$	75	6	7
V	SSA22	15.7	$V < 24.5$	172	43	15
	HDF	14.3	$V < 23.75$	87	15	6
I	SSA22	15.7	$I < 23.25$	196	50	25
	SSA13	12.8	$I < 22.5$	95	14	5
K	SSA22	15.7	$K < 20.5$	109	37	24
	HDF	14.3	$K < 20.5$	96	15	29
	SSA13	12.8	$K < 20$	83	12	22
	SSA4	14.9	$K < 19$	49	25	17

Table 2. Fits to 2000 Å Luminosity Functions

z Range	α	M_* ^a	ϕ_* ($\times 10^{-3}$ Mpc $^{-3}$)	L ($\times 10^{26}$ ergs cm $^{-2}$ s $^{-1}$ Hz $^{-1}$)
1.0 – 1.5	–1.0	-19.1 ± 0.25	10.0	1.8
	–1.5	-19.3 ± 0.15	0.8	2.5
0.5 – 0.9	–1.0	-18.2 ± 0.3	16.0	1.2
	–1.5	-18.5 ± 0.4	11.0	1.4
Local ^b	–1.6	$-19.16^{+0.31}_{-0.29}$	2.5	0.7

^aErrors in M_* are 98% confidence limits except for the local value, for which errors are 1 σ . All values are calculated for $H_0 = 65$ km s $^{-1}$ Mpc $^{-1}$ and $q_0 = 0.5$.

^bTreyer et al. (1998)

Fig. 1.— Sky surface brightness of the integrated galaxy light in the Hubble Deep Field. The solid line shows the integrated light from all the galaxies, the filled squares that of known $z < 1$ galaxies, and the filled diamonds that of $z < 0.5$ galaxies. The dashed line shows the light from galaxies known to be at $z > 1$ plus all unidentified galaxies.

Fig. 2.— Absolute 2500 Å rest-frame magnitudes versus redshift, computed from the U' (filled squares), B (open diamonds), V (stars), and I (filled triangles) samples.

Fig. 3.— Luminosity functions in the redshift interval $0.7 < z < 1.3$ constructed at rest wavelengths of 1700 Å (open diamonds), 2250 Å (filled squares), and 2750 Å (open triangles) from the U' , B , and V samples, respectively.

Fig. 4.— Luminosity density in the redshift interval $0.7 < z < 1.3$ computed from the luminosity functions of Fig. 3. The squares are the luminosity density for galaxies with luminosity $M_{AB} > -17.5$. The thin dashed line represents a power law fit to the data. The solid line is $2.6 \times 10^{26} (\lambda/3000 \text{ Å})^{1.1} \text{ ergs cm}^{-2} \text{ s}^{-1} \text{ Hz}^{-1}$, which represents the power law fit to the luminosity densities extrapolated to $M_{AB} = -16$, assuming an $\alpha = -1$ Schechter function.

Fig. 5.— 2500 Å rest-frame luminosity function (diamonds and solid line) in the redshift interval $0.2 < z < 0.5$ constructed from the U' sample. $\pm 1 \sigma$ error bars are shown. The dotted line is the luminosity function computed from only the observed objects (the “minimal” function), whereas the dashed line is computed after placing all of the unidentified objects into the redshift bin (the “maximal” function).

Fig. 6.— As in Fig. 5 but for the redshift interval $0.6 < z < 1.0$, constructed from the B sample.

Fig. 7.— As in Fig. 5 but for the redshift interval $1.0 < z < 1.5$, constructed from the V sample.

Fig. 8.— $M_U < -16$ light density at 2500 Å as a function of redshift: directly determined in the interval $0.2 < z < 0.5$ and incompleteness-corrected via an $\alpha = -1$ Schechter function for the intervals $0.6 < z < 1.0$ and $1.0 < z < 1.5$. In each redshift interval the light density is shown as a filled square and the redshift range as a thin horizontal line. Statistical and systematic errors (Appendix) are shown as the thick portions of the error bar. Light densities computed using the minimal and maximal functions (see text and Figs. 5 – 7) are shown as open squares joined by thin vertical lines. The solid line is a $(1 + z)^{1.5}$ evolution law. The dashed line shows an evolution of $(1 + z)^4$, normalized to the second data point.

Fig. 9.— 2500 Å rest-frame luminosity functions ($q_0 = 0.05$) for the redshift intervals

$0.20 < z < 0.50$ (filled diamonds), $0.60 < z < 1.00$ (filled triangles; offset by +0.65 mag relative to the $[0.20, 0.50]$ function), and $1.00 < z < 1.50$ (open triangles; offset by +0.75 mag relative to the $[0.20, 0.50]$ function).

Fig. 10.— 2000 Å rest-frame luminosity function in the redshift interval $0.5 < z < 0.9$ (filled diamonds and solid line), computed from the U' sample, compared with the luminosity function constructed from the local rest-frame UV-selected sample of Treyer et al. (1998) (dashed line) for $H_0 = 65 \text{ km s}^{-1} \text{ Mpc}^{-1}$. The latter has been renormalized upward by a factor of 1.7 to match the $z = 0.7$ luminosity function.

Fig. 11.— As in Fig. 10 for the redshift range $1.0 < z < 1.5$, constructed from the B -selected sample. Here the local UV luminosity function of Treyer et al. (1998) has been multiplied by a factor of 2.8 to match the $z = 1.25$ function.

Fig. 12.— Incompleteness-corrected rest-frame 2000 Å luminosity densities to $M_{AB} = -16$ in the redshift intervals $0.5 < z < 0.9$ and $1.0 < z < 1.5$ (filled squares), constructed from the luminosity functions of Figs. 10 and 11, compared with the measured 2000 Å luminosity density from the local Treyer et al. (1998) sample (filled diamond), for $H_0 = 65 \text{ km s}^{-1} \text{ Mpc}^{-1}$ and $q_0 = 0.5$. This number has been computed for the range $M_{AB} < -16$ only. Thin horizontal lines show the redshift ranges. For the present data, the open squares show the densities computed with the minimal and maximal functions (see text and Figs. 5–7), joined by thin vertical lines. Statistical and systematic errors (Appendix) are shown by thick vertical lines. The solid line is a $(1+z)^{1.5}$ evolution line, while the dashed line is a $(1+z)^4$ evolution, normalized to the $z = 0.7$ point.

Fig. 13.— Incompleteness-corrected rest-frame 2800 Å luminosity density as a function of redshift. Filled squares show the densities from the present work for the redshift intervals $0.2 < z < 0.5$ (constructed from the U' sample), $0.5 < z < 0.75$ (from the B sample), $0.75 < z < 1$ (from the V sample) and $1.0 < z < 1.5$ (also from the V sample). The filled diamond is the density constructed from the Treyer et al. (1998) sample corrected to 2800 Å, the open diamonds are Lilly et al.’s (1996) “LF-estimated” total 2800 Å densities from the CFRS survey, and the open triangles show the densities derived from Connolly et al. (1997) (upright symbols) and Sawicki et al. (1997) (inverted symbols), scaled downwards by 20% as discussed in the text. $H_0 = 65 \text{ km s}^{-1} \text{ Mpc}^{-1}$ and $q_0 = 0.5$. The dashed line shows a $(1+z)^4$ evolution law, similar to the $(1+z)^{3.9 \pm 0.75}$ law derived in Lilly et al. (1996). Thin horizontal lines show the redshift intervals in all cases. For the present data, open squares show the densities constructed from the minimal and maximal functions (see text and Figs. 5–7), connected by thin vertical lines. Thick vertical lines show the statistical and systematic errors (Appendix).

Fig. 14.— 8000 Å rest-frame luminosity functions in the redshift intervals $0.2 < z < 0.5$ (filled diamonds and dotted line), constructed from the *I*-selected sample, and $0.7 < z < 1.3$ (filled squares and solid line), constructed from the *K*-selected sample. $\pm 1 \sigma$ errors are shown at each point.

Fig. 15.— *V*-band number counts (galaxies plus stars) in the HDF proper (small squares) and in the HDF flanking fields region (large symbols). The dashed line is a power-law fit to the bright-end data.

Fig. 16.— *B*-band galaxy counts from the HDF proper (Williams et al. 1996; small squares) compared with the average *B*-band galaxy counts in the regions of the HDF and SSA22 used in the present work (large symbols). Spectroscopically confirmed stars have been removed in both cases.

Fig. 17.— Comparison of sky surface brightnesses of galaxies in the HDF proper (filled symbols and solid line) with those in the much larger flanking fields. The integration excludes known stars and is over the *AB* magnitude range 21 – 24.25 in the red, 21 – 24.5 in the visual, and 21 – 24.75 in the blue. The solid line shows the total sky surface brightness for the HDF proper for comparison with the large open squares, which show this for the flanking fields. The smaller squares are for known $z < 1$ galaxies and the smaller diamonds for $z < 0.5$ galaxies. The dashed line shows the possible $z > 1$ light for this magnitude range.

Fig. 18.— Rest-frame 2500 Å luminosity functions in the redshift range $0.6 < z < 1.0$ constructed from subsamples of the *B*-selected sample: the HDF plus SSA22 data (filled squares and dashed line) and the SSA13 plus SSA4 data (open squares and solid line). Error bars are $\pm 1 \sigma$.

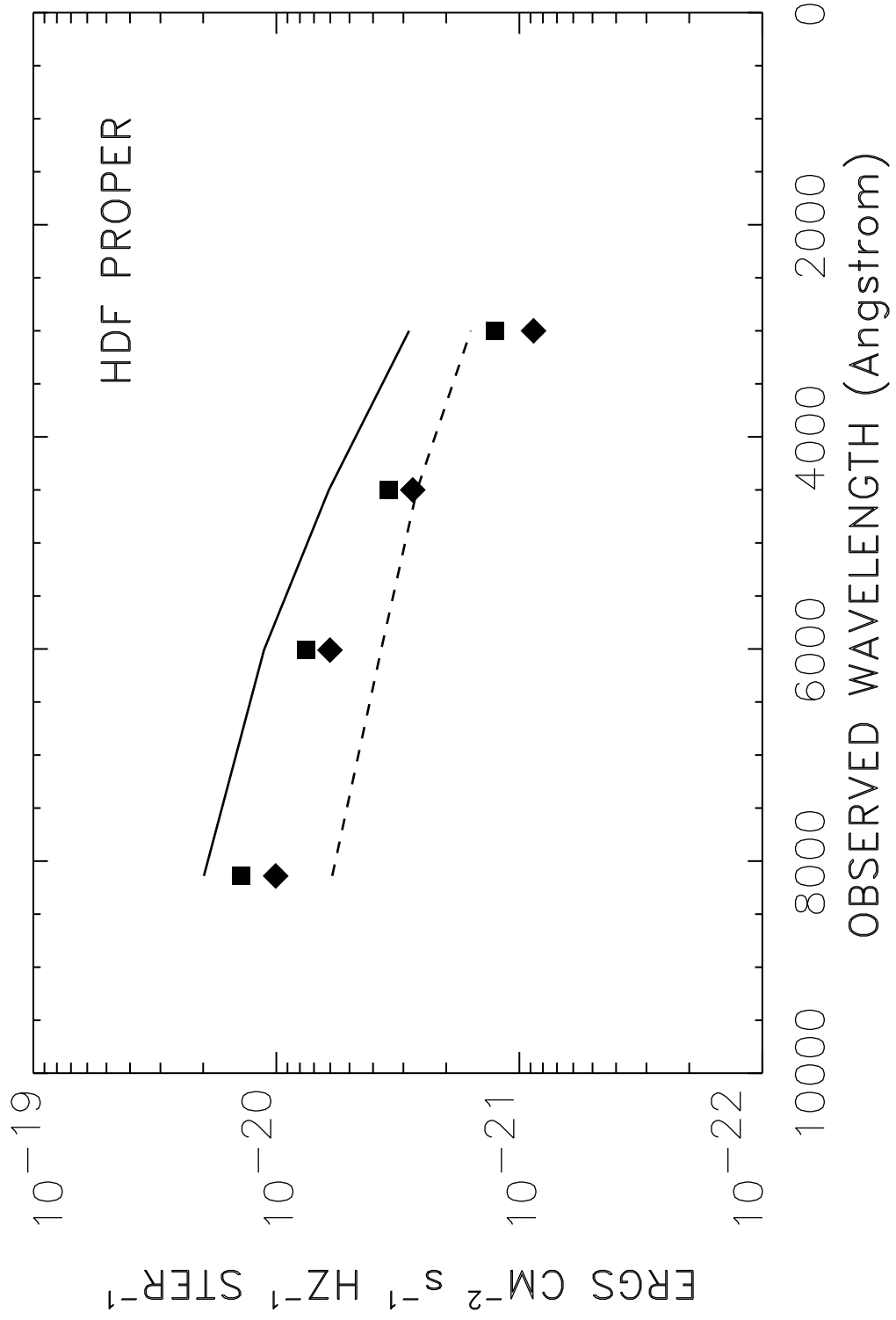


Fig. 1.—

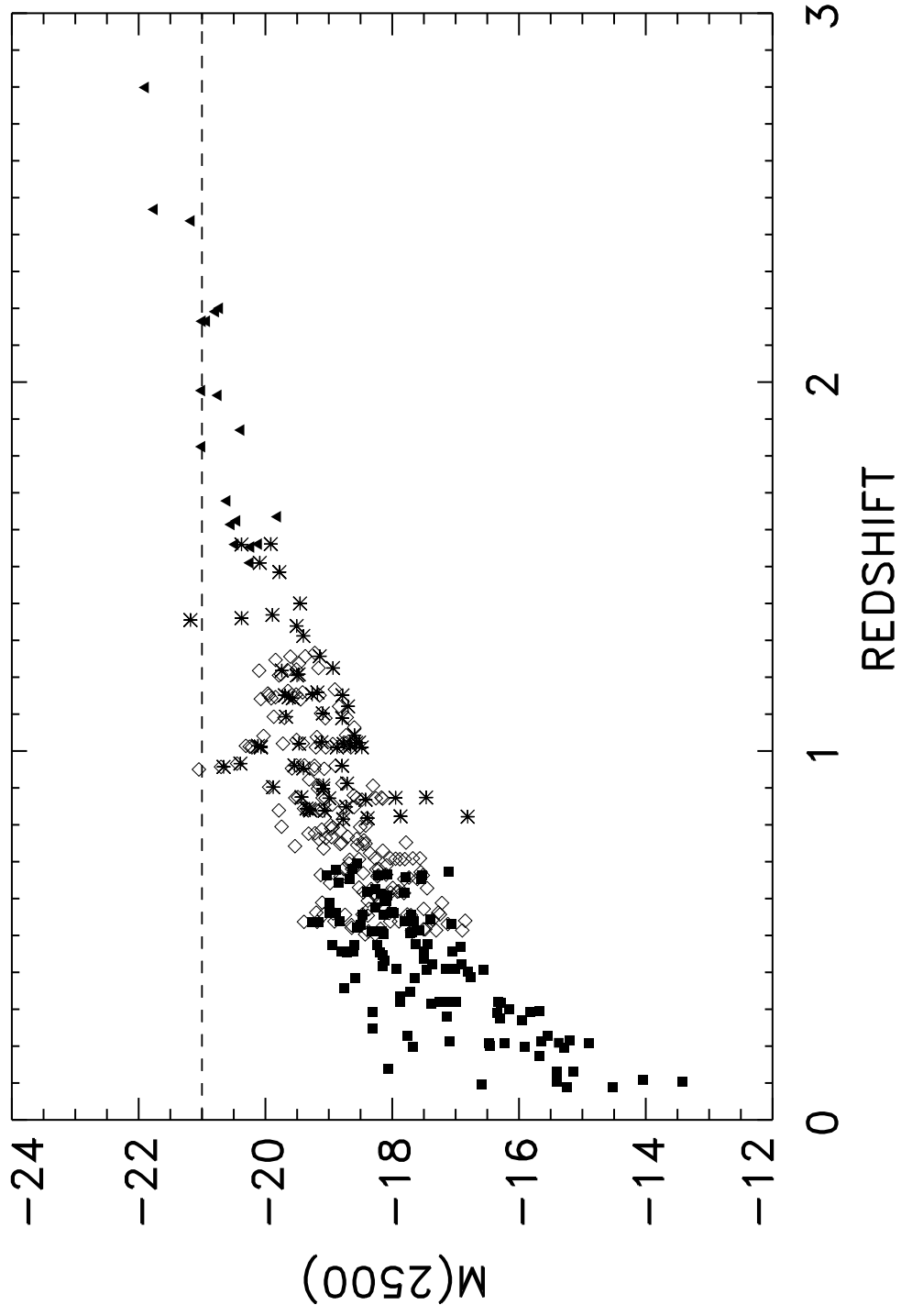


Fig. 2.—

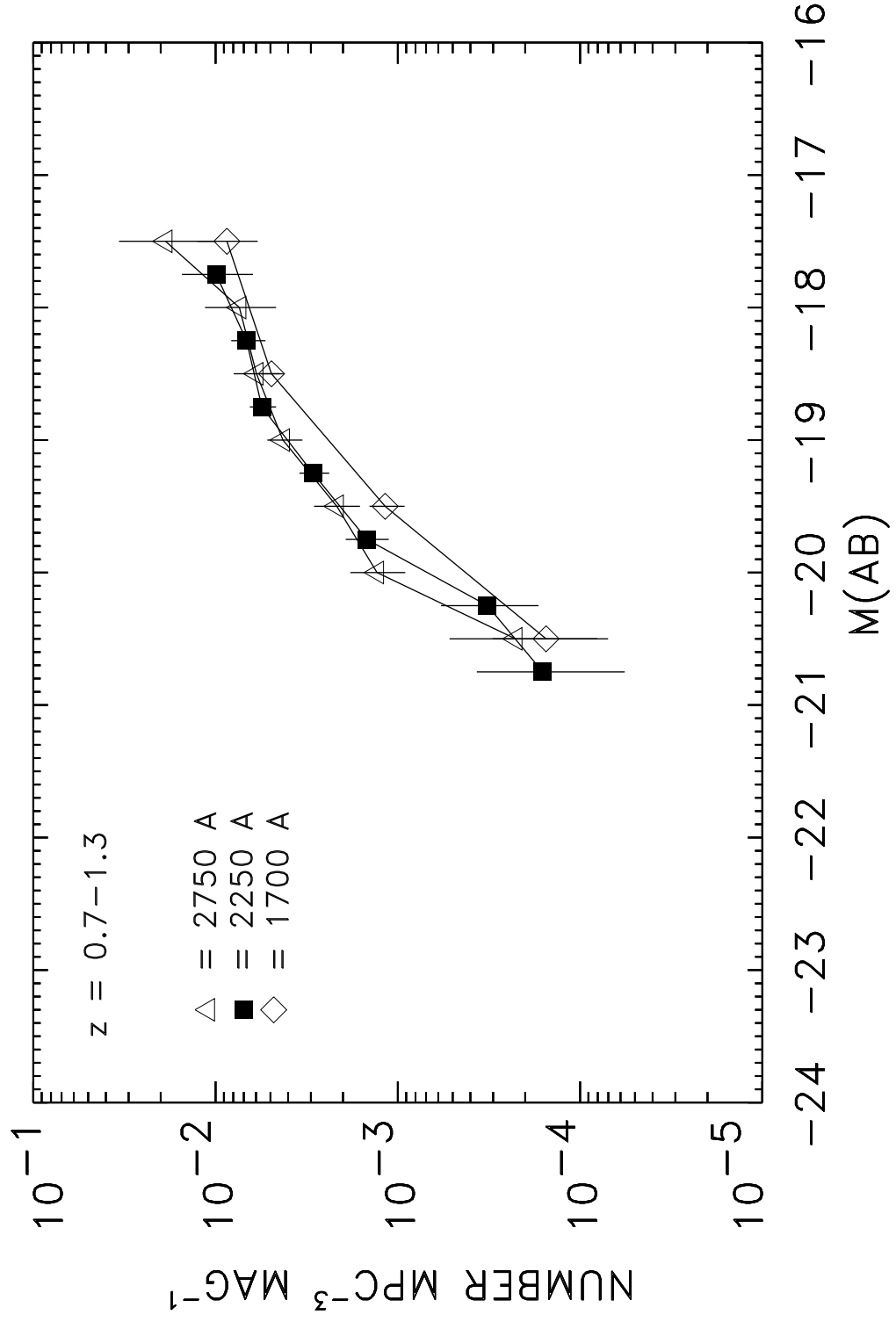


Fig. 3.—

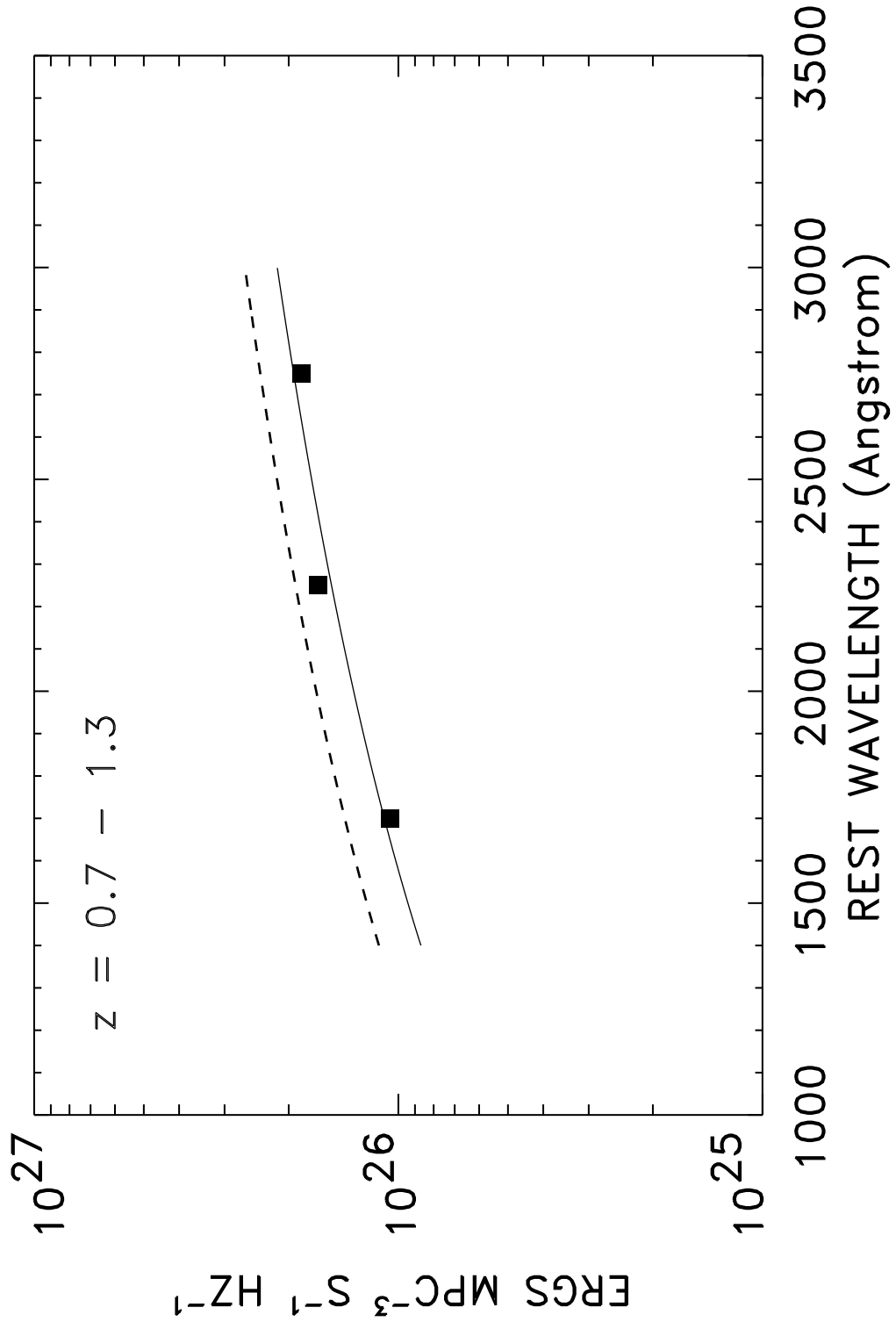


Fig. 4.—

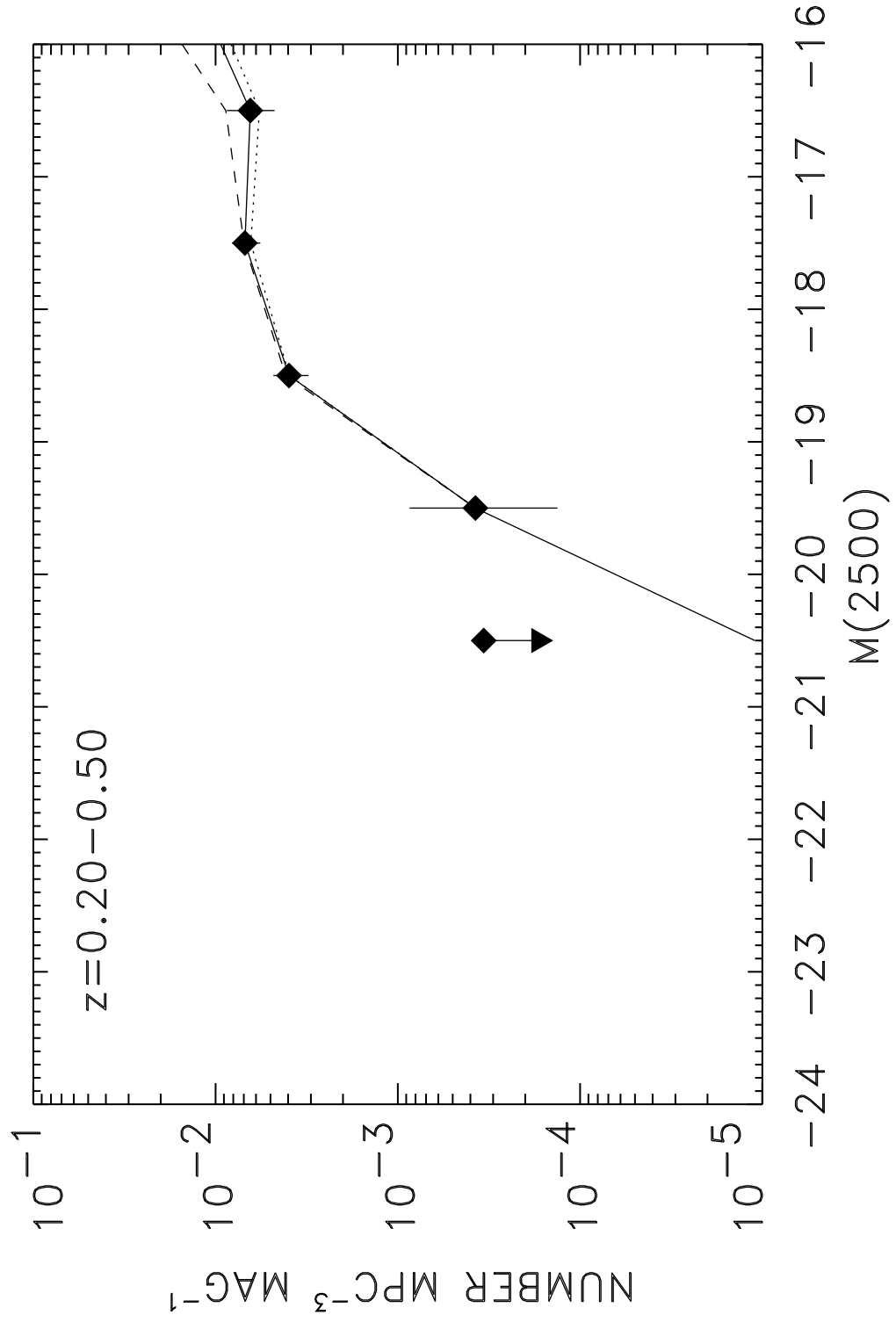


Fig. 5.—

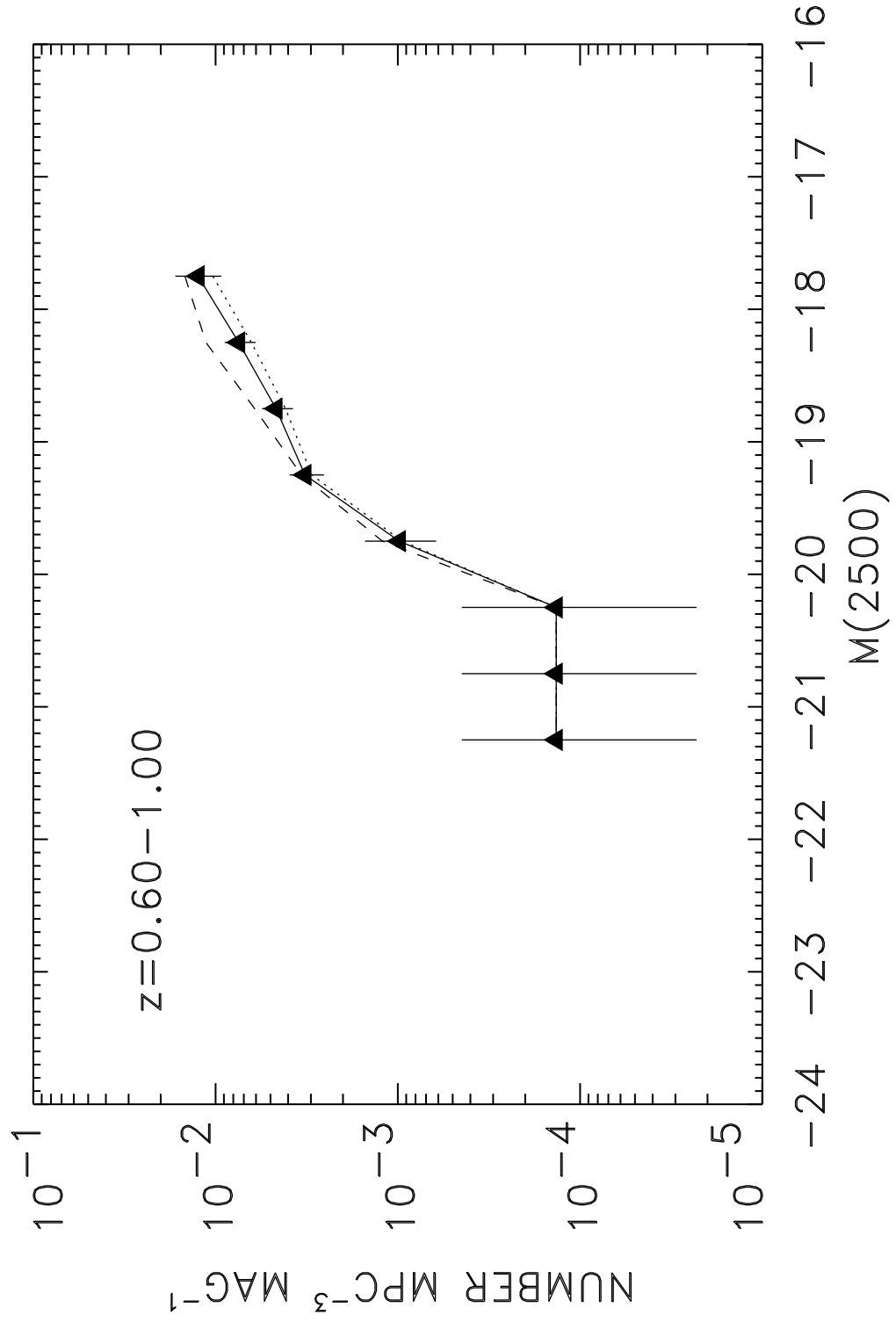


Fig. 6.—

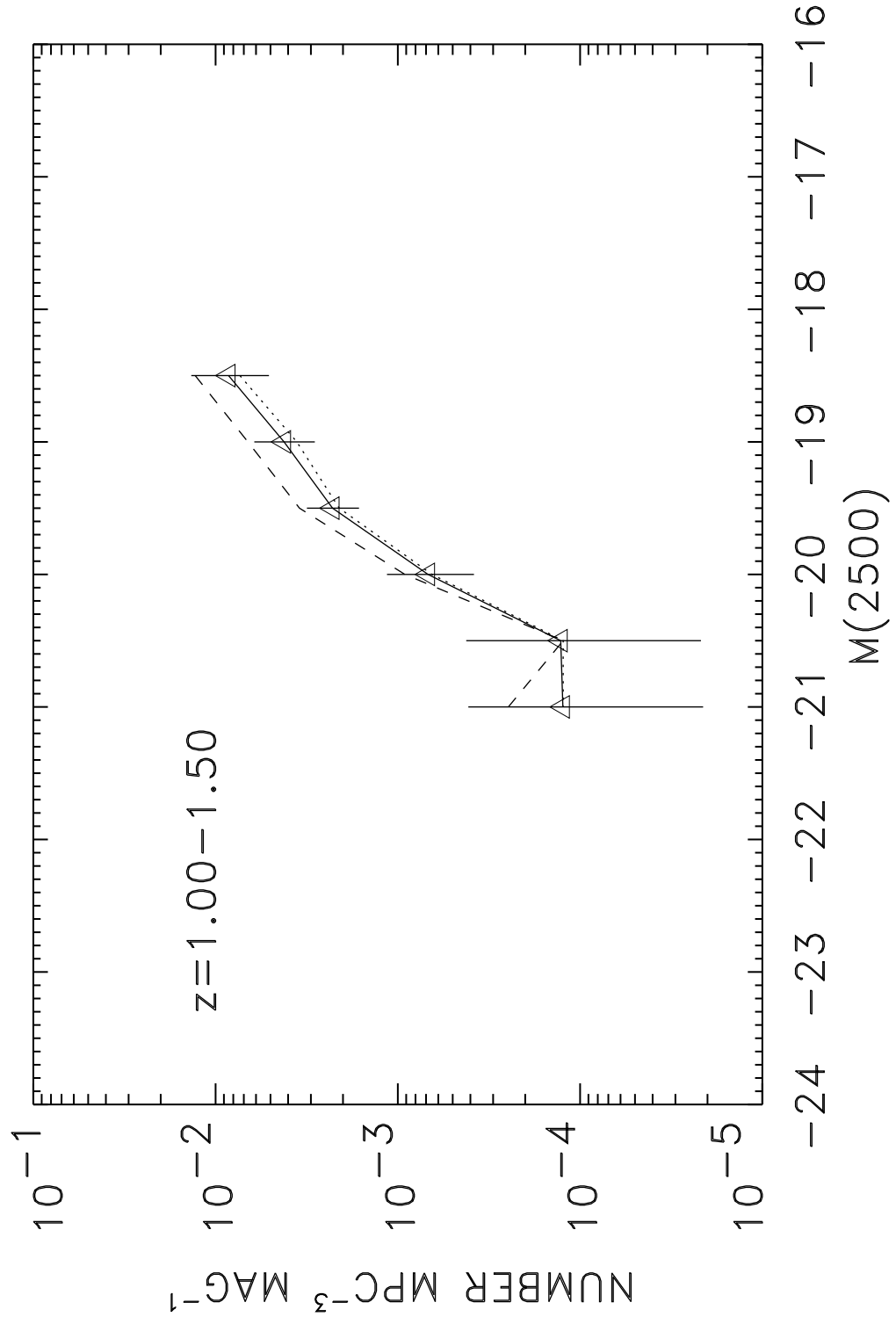


Fig. 7.—

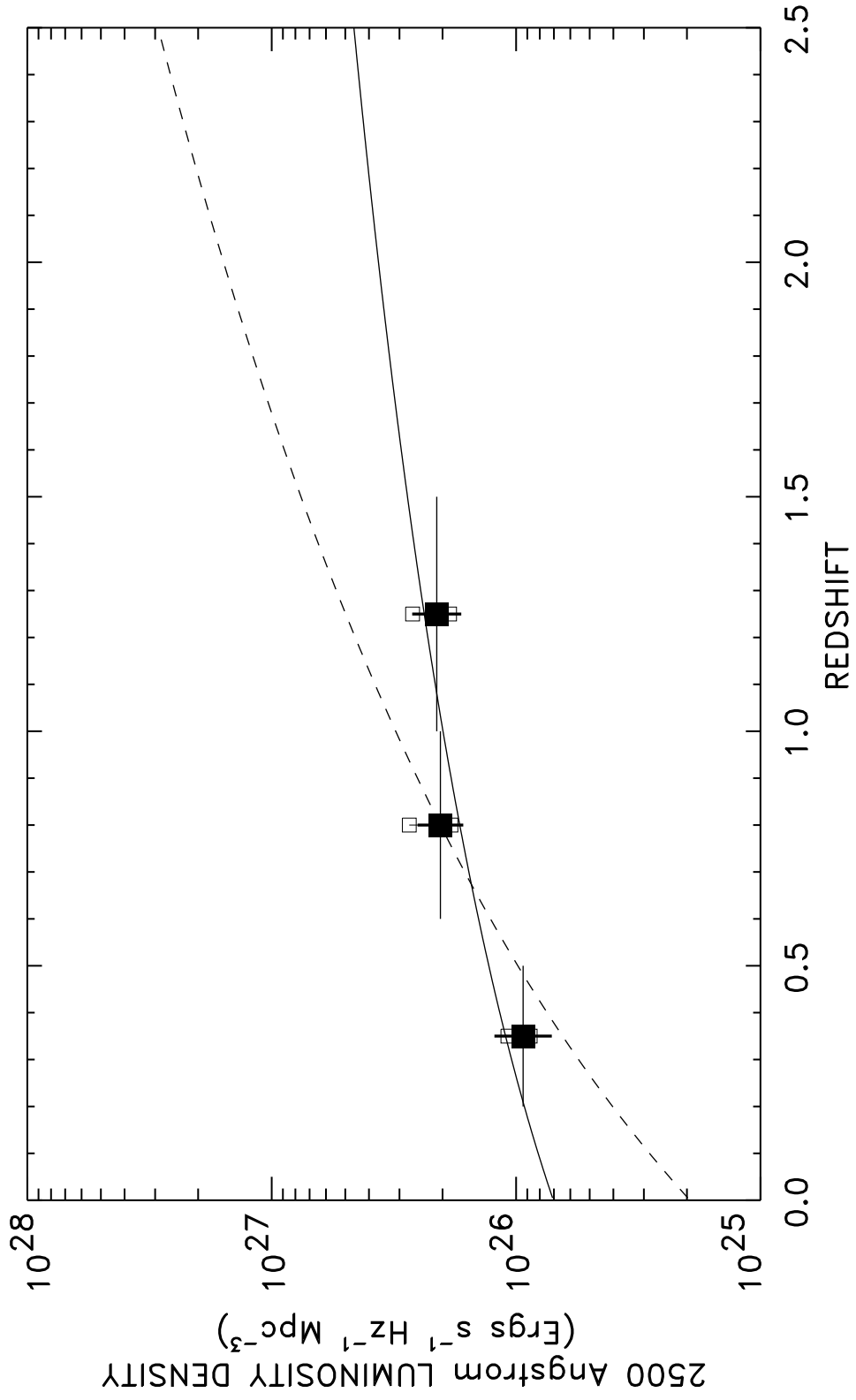


Fig. 8.—

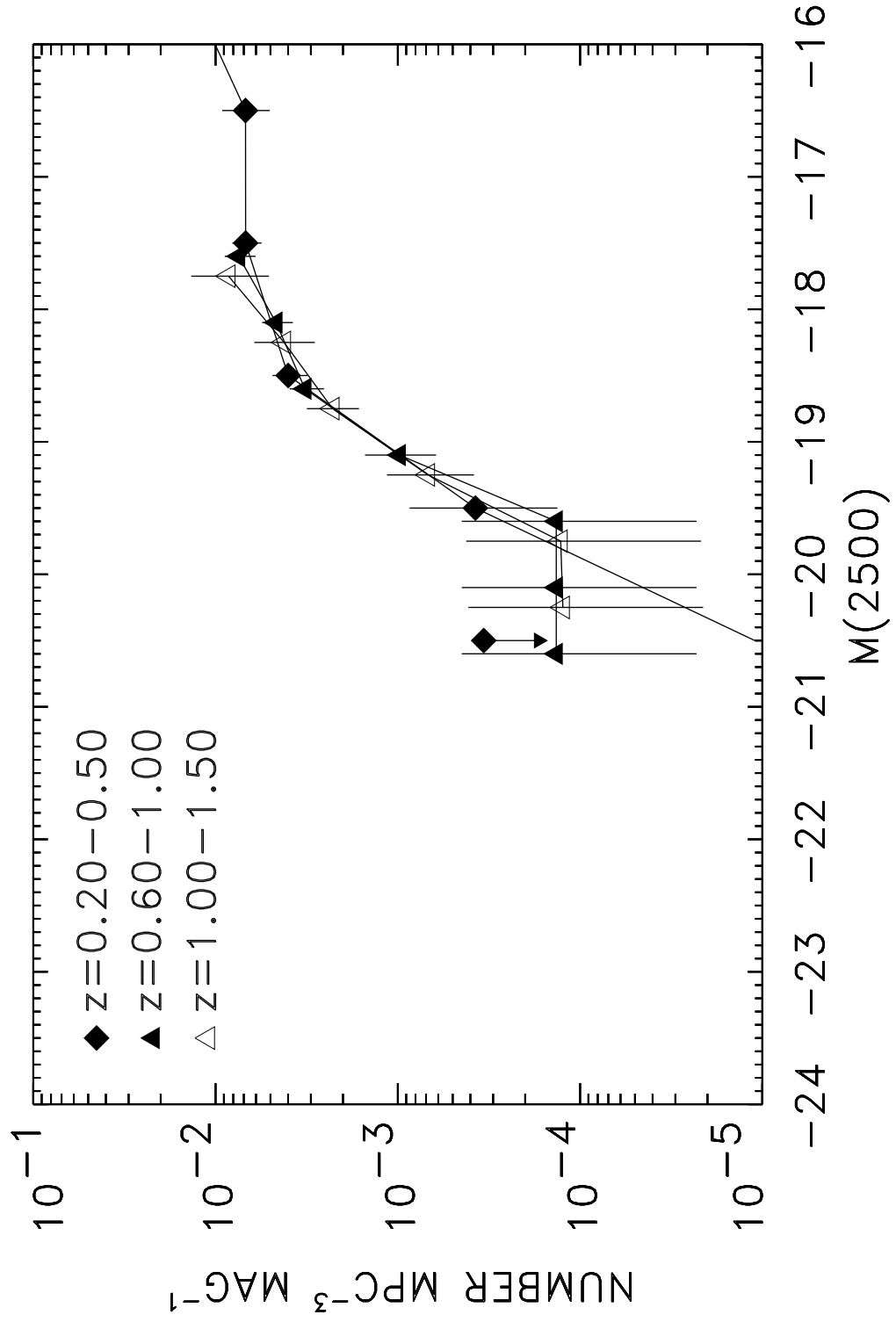


Fig. 9.—

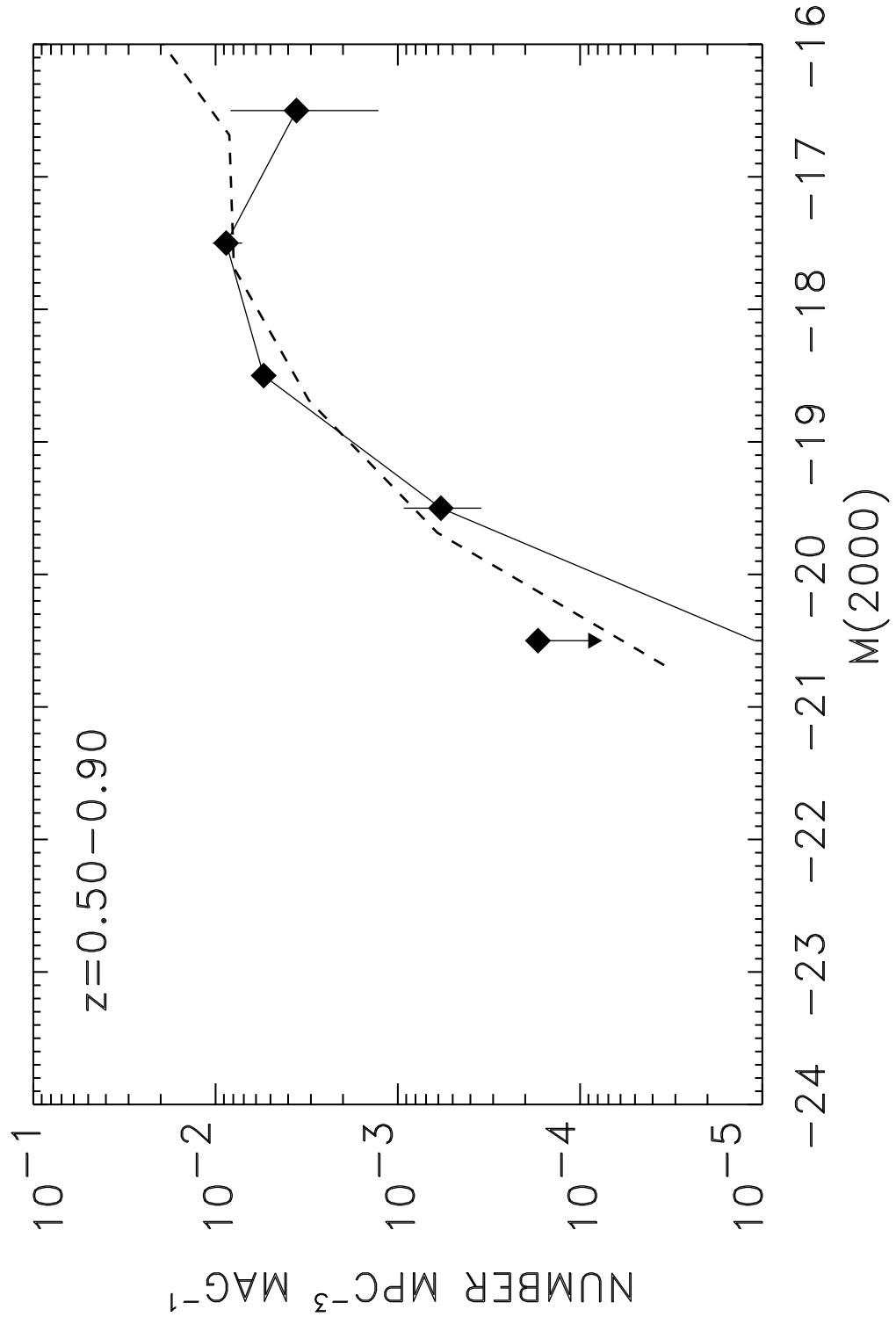


Fig. 10.—

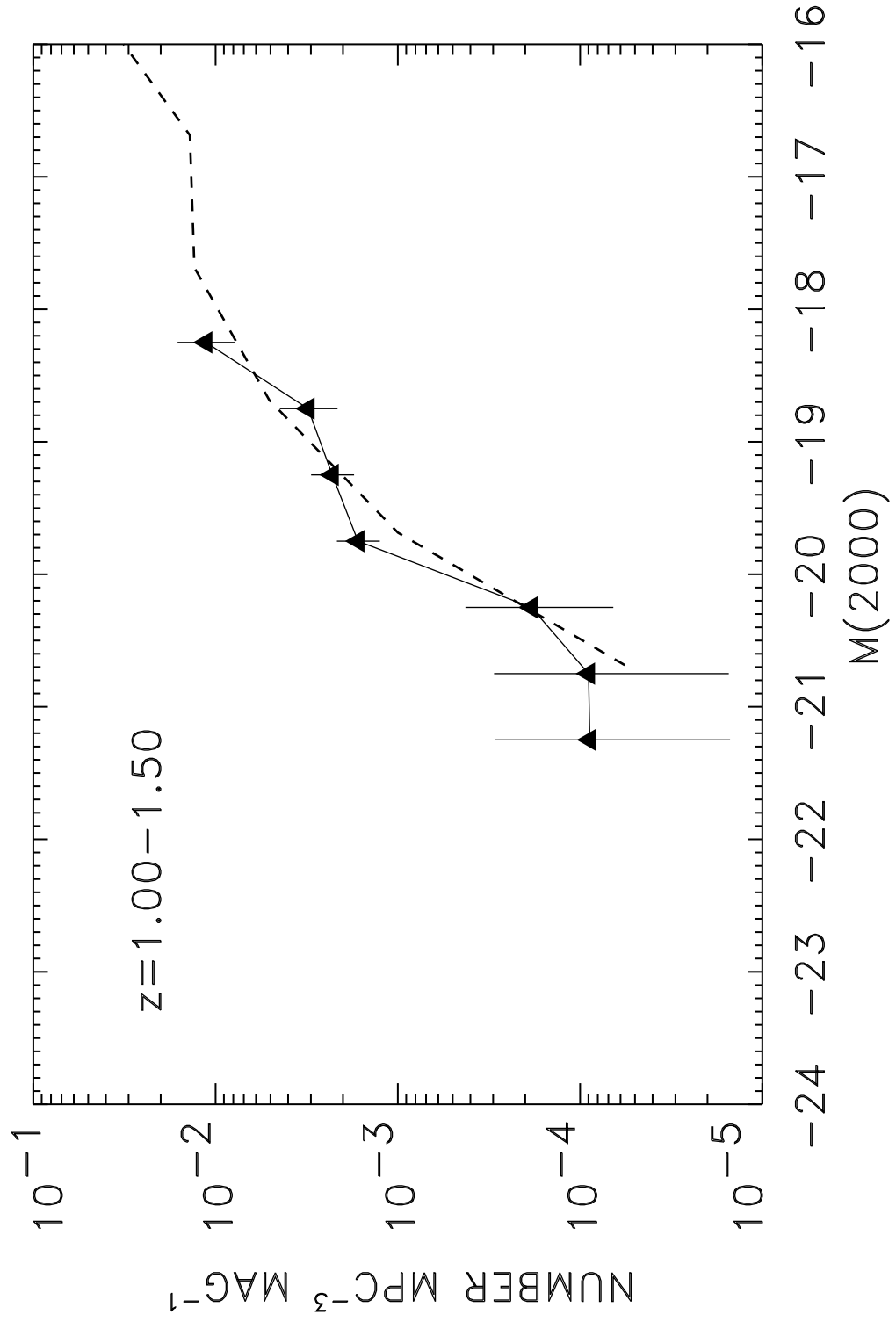


Fig. 11.—

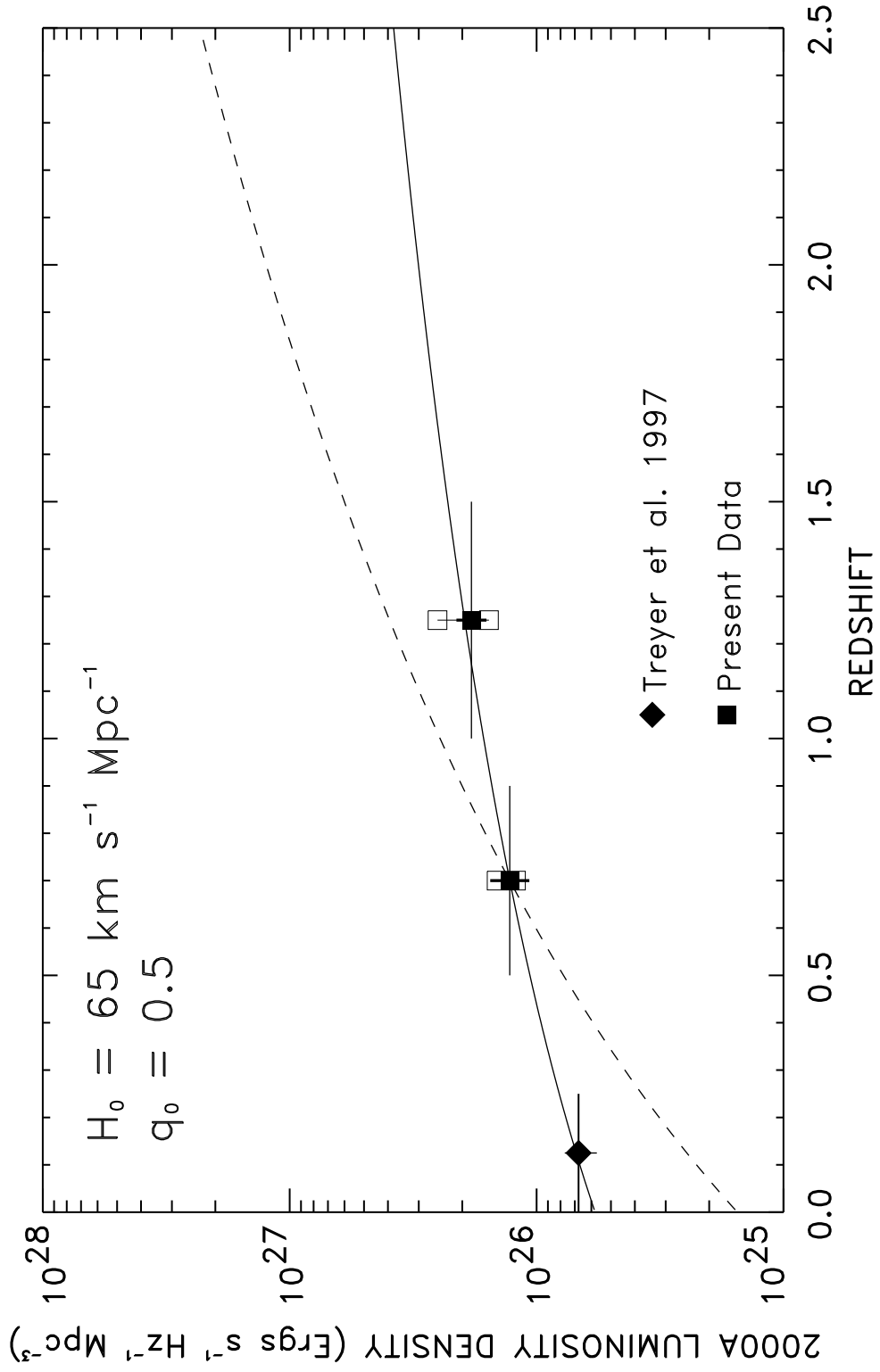


Fig. 12.—

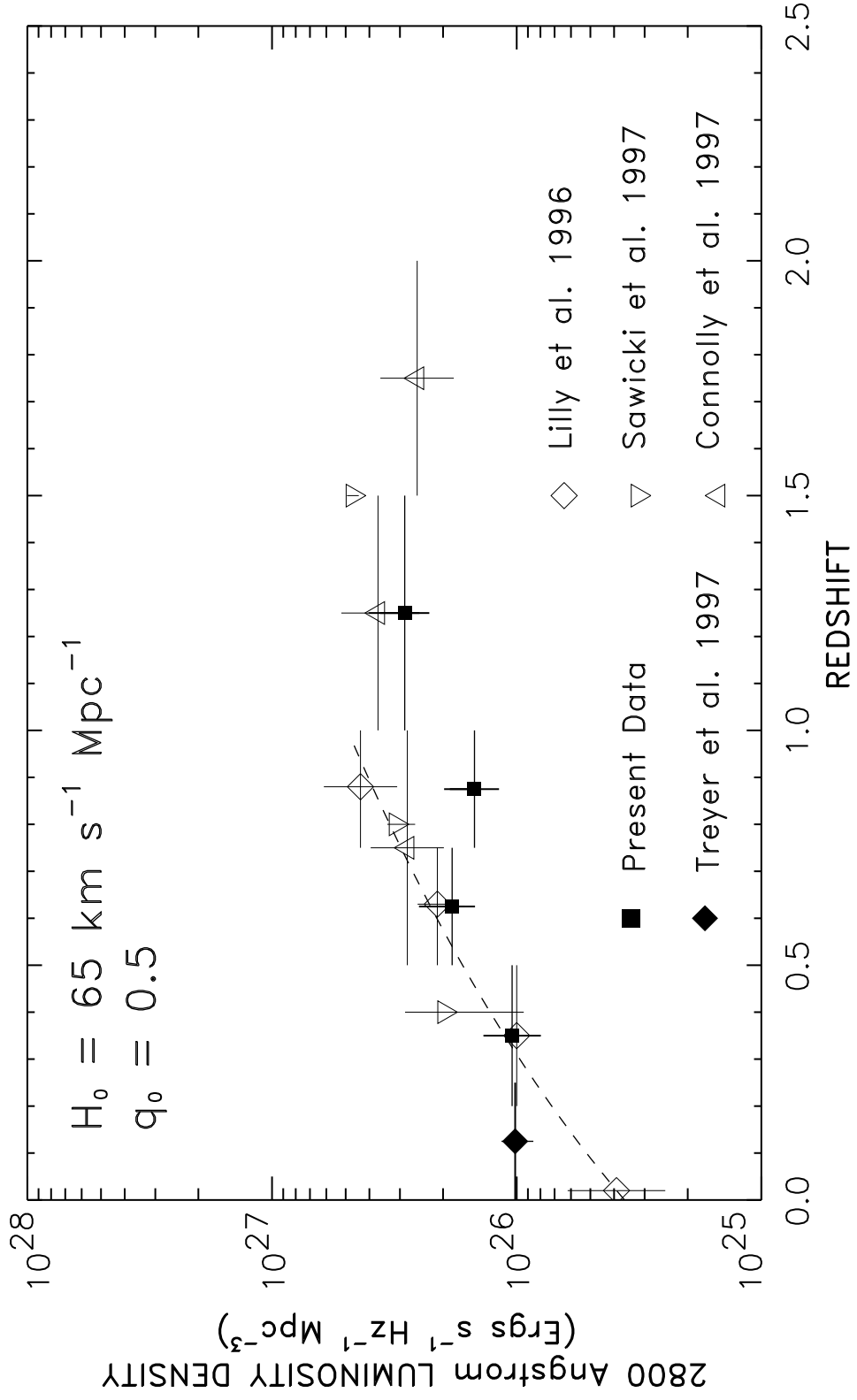


Fig. 13.—

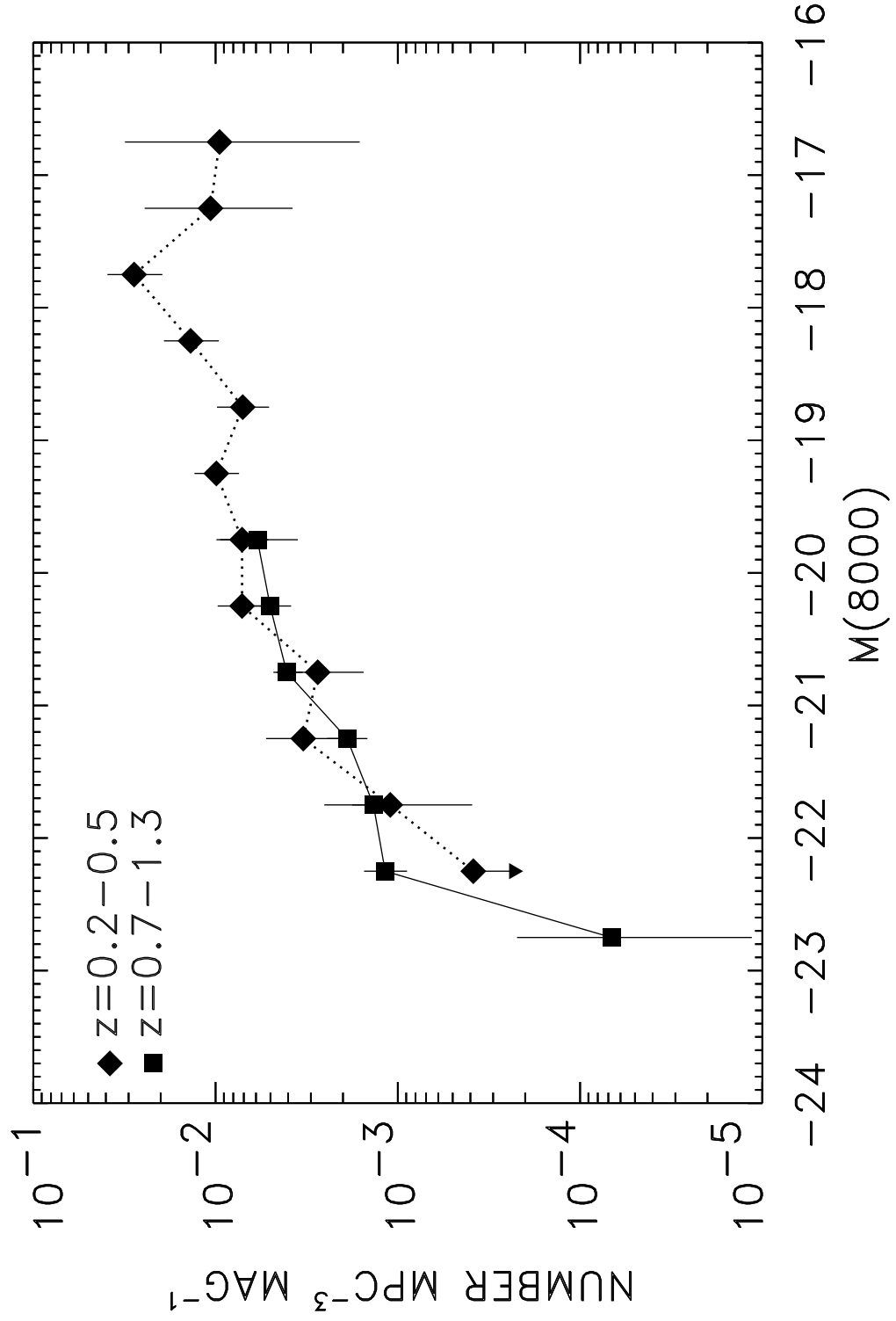


Fig. 14.—

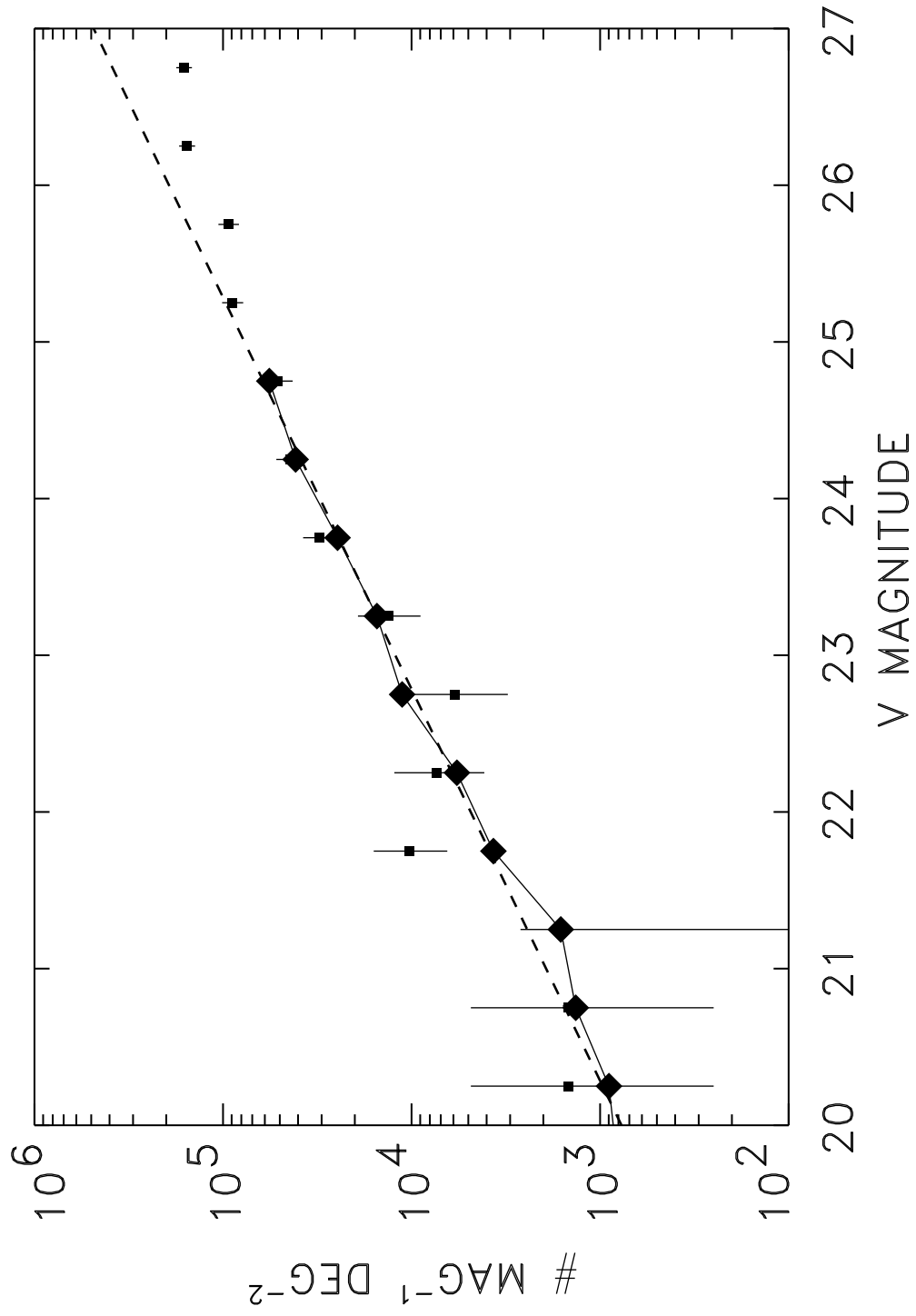


Fig. 15.—

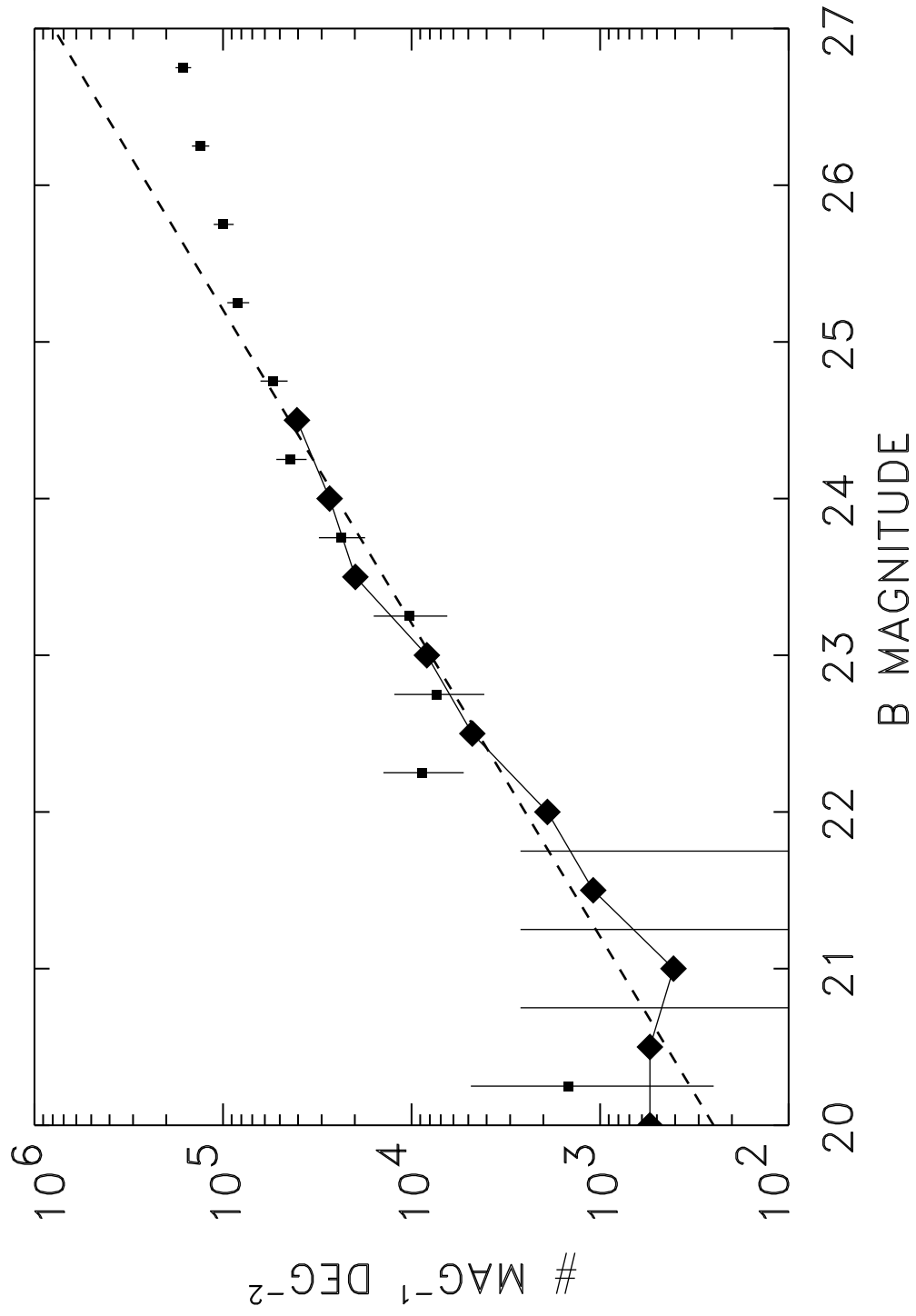


Fig. 16.—

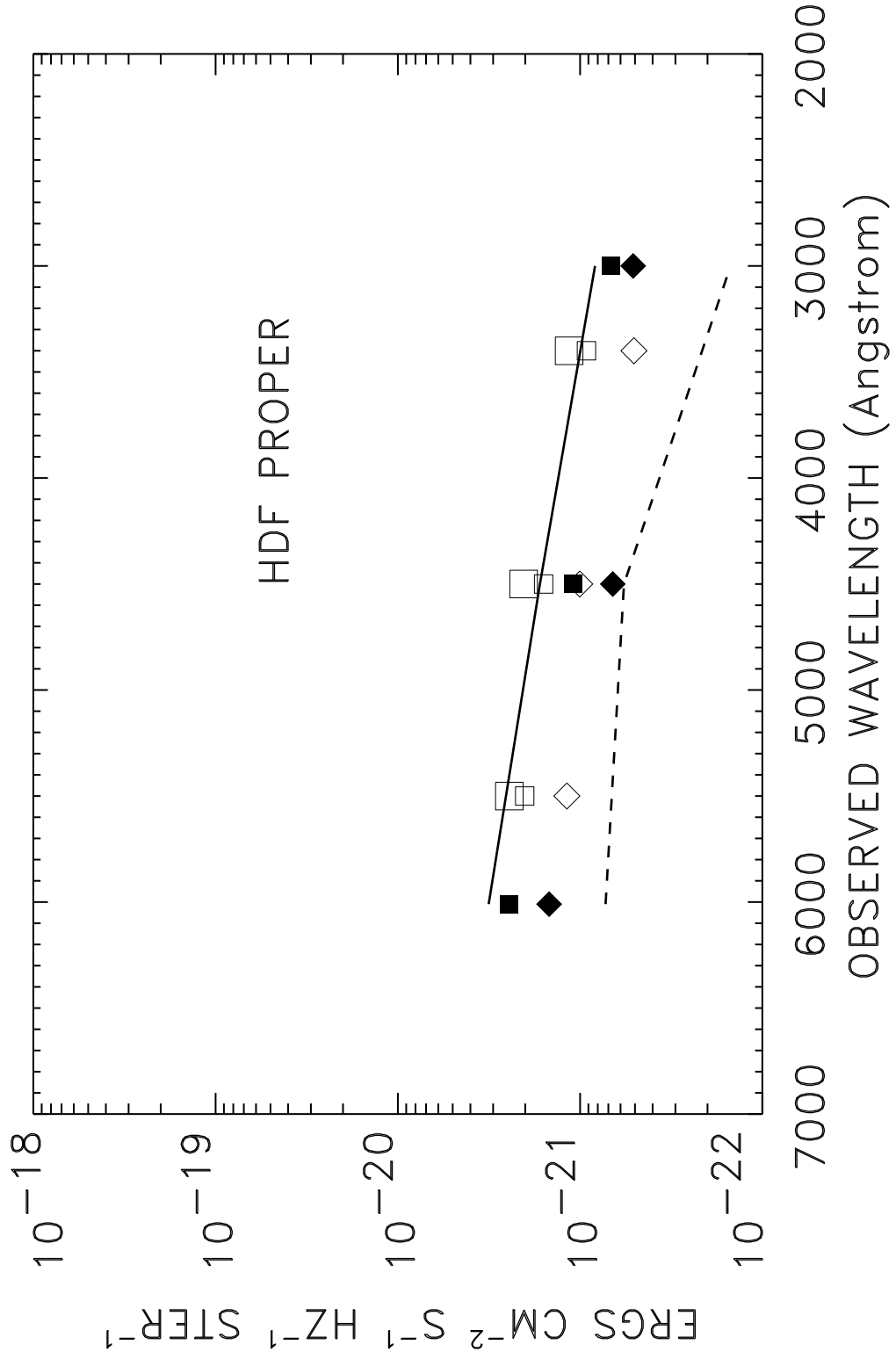


Fig. 17.—

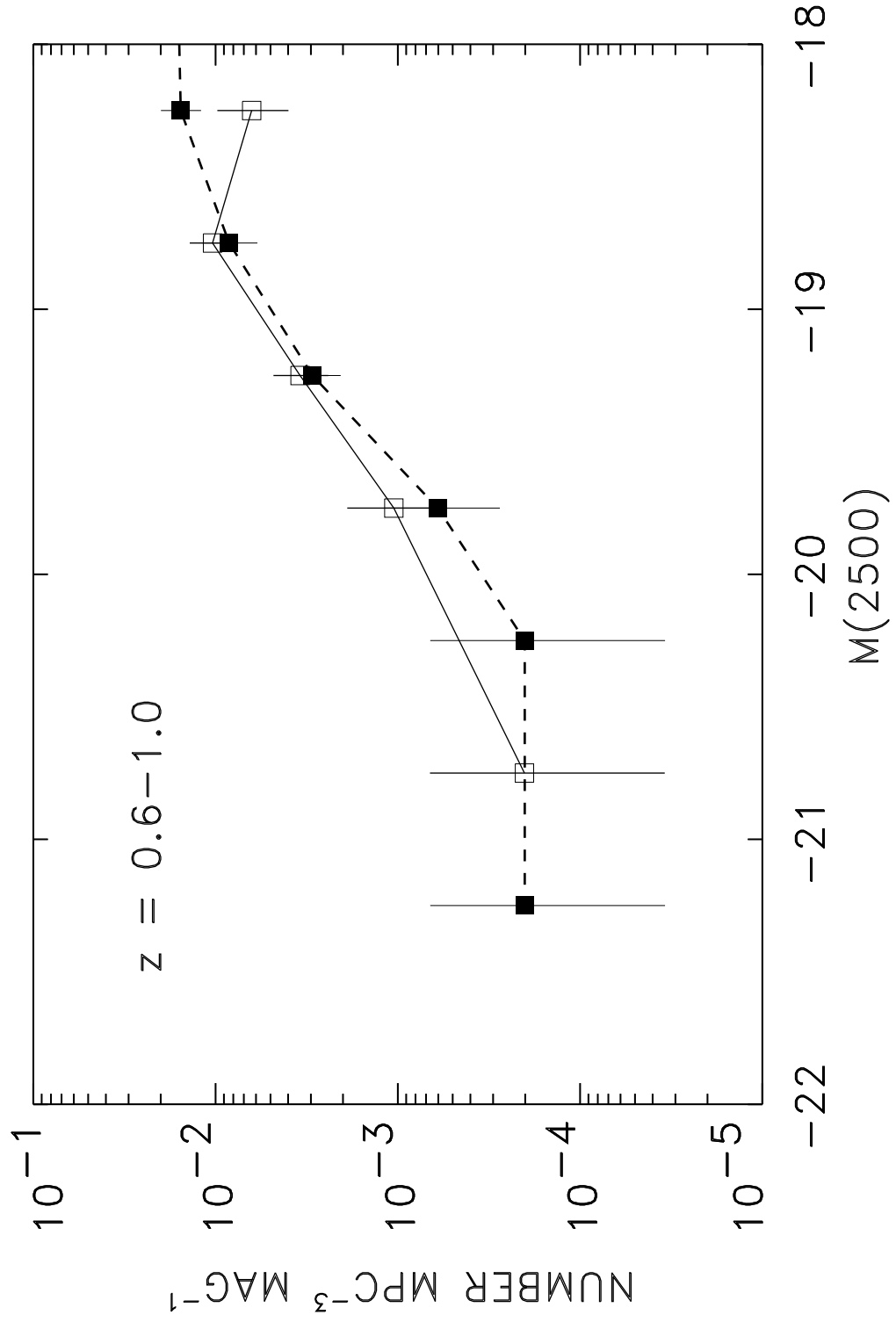


Fig. 18.—